

## Back-calculation of the 2017 Piz Cengalo-Bondo landslide cascade with r.avaflow

*Martin Mergili, Michel Jaboyedoff, José Pullarello, Shiva P. Pudasaini*

### Response to the comments of Referee #1

We would like to thank the reviewer for the constructive remarks. Below, we address each comment in full detail. Our response is written in blue colour. **Changes in the manuscript are highlighted in yellow colour.**

The authors present an application of the model r.avaflow to the back-calculation of a complex landslide occurred in Switzerland. The case-study is indeed interesting and the scientific question about the two scenario is stimulating (I also really like fig.5). However, as you stated yourself, the investigation of the process through a two-phase numerical model did not allow to discern between the two scenario. So what is really the “take home message” of your work? I do understand that negative results are results but in a way you do not really present them as such. For example, most of your introduction praise the capabilities of two phase depth averaged model in “support the confirmation or rejection of conceptual models” stating the intrinsic epistemological potentiality with respect to one phase models. However, you then proceed with your modelling, that anyhow requires calibration and the selection of vague “physical plausible” parameters, that has numerical issues that constrain you to use “physically implausible” parameters and that do not perform well in the reconstruction of the actual phenomenon. So rather than titling your paper as “back calculation of the 2017: : :” I would suggest to switch it to something such as “challenges and open issues regarding the modelling of the 2017: : :”.

Confirmation and rejection of conceptual models is probably too much emphasized in the introduction of the discussion paper – in fact it is not the main aim of the work to find out which of the two scenarios is the “winner”, but rather to investigate on how well the two scenarios can be reproduced, and what are the main challenges in doing so. The observation of the reviewer that we cannot find out the “winner” scenario while having to optimize the parameters is absolutely correct. We have reformulated the introduction and extended the discussion accordingly (confirmation and rejection of conceptual models are now treated in the discussion, L343–345):

*Confirmation or rejection of conceptual models with regard to the physical mechanisms involved in specific cases would have to be based on better constrained initial conditions, and the availability of robust parameter sets.*

The title, in contrast, is appropriate as it is, we think. The results are far from perfect, of course, but, still, most of the characteristics of the flow can be “reasonably” (see response below) reproduced, and this is only possible with particular two- or multi-phase models – aspects which are discussed in more detail in the revised manuscript (see e.g. L357–372).

These are my other comments regarding your paper

BROAD COMMENTS

1) Optimization and equifinality: The entrainment in your code is calculated with a calibrated coefficient and based on a depth averaged kinetic energy. You defined 6 zones with different friction angles and other calibrated coefficient. How did you suppose it could lead to a selection to confirm or reject a conceptual model (I 51) when, as you stated yourself in the end, there is an obvious problem of equifinality? This issue is common in back analysis, especially when several parameters are involved in the calibration process. To try to give some “physical plausibility” to the whole parametrization of the backward calculation it is important to:

i) define a straightforward and explicit optimization method

ii) use parameters that are somewhat geotechnically believable with respect to the observed phenomena

iii) provide a clear geomorphological/mechanical reason for each zonation – otherwise of course the more are the zones in which the parameters may be changed, the more the equifinality issue arises.

In my opinion point i) is lacking in your paper. The metrics you use are not so straightforward, especially if you need to jump between two papers to reach their definition and reason of being (is it really Mergili 2018b the best paper to refer to or is it better to go directly to Formetta 2015 and Mergili et al., 2017?). Please devote a paragraph to the interpretation of these metrics rather than cut the discussion off with “indicators of a reasonably good corrispondance”. And what is reasonably anyway? Please also show in the picture a zoom of the deposition pattern (modelled and observed) in the alluvial fan. Point ii) is also important. Finding a 45 angle of friction in the E zone is rather “physically un-plausible” as it is, especially when your solid fraction decreases. You discuss this too briefly in the end of the discussion chapter. You have to explain better what is the issue with the code, is the 10 m sampling? is a projection issue related to the conversion of the coordinates? This should be better discussed, also in the light of the new titling of the manuscript. The zoning (point iii) should be more extensively discussed, the definition that it is found in table 1 is too synthetic. For each zone and limit there must be a defined reason to be it that way.

Thank you very much for this detailed and comprehensive comment. It helps us to better formulate some of the main points and challenges of the work:

- Straightforward and explicit (automated) optimization method: in principle, such methods exist in the literature (e.g. Fischer, 2013) and are available to the authors. However, they have been developed for optimizing globally defined parameters (which are constant over the entire study area) against runout length and impact area, and such tools do a very good job for exactly this purpose. However, they cannot directly deal with spatially variable parameters, as they are defined in the present work. With some modifications they might even serve for that – but the main issue is that optimization also considers shapes and maximum values of hydrograph discharges, or travel times at different places of the path. It would be a huge effort to trim optimization algorithms to this purpose, and to make them efficient enough to prevent excessive computational times – we consider this as an important task for the future which is out of scope of the present work. Therefore, we have to use a step-wise expert-based optimization strategy. This is discussed accordingly in the revised manuscript. Regarding the reference parameter set,

we still think that Mergili et al. (2018b) is most appropriate, as it is newer than the other papers, therefore based on more experience and a newer version of the software, and closest to the Piz Cengalo-Bondo event in terms of process type (even though much higher in magnitude).

- Plausibility of parameters: the 45° friction angle would only apply if the flow would consist of pure solid. In the simulation, it is reduced linearly with the fluid fraction. As the fluid fraction is commonly >50% in Zone E, the friction angle of the solid is <20°. This aspect, which helps to adapt the effective characteristics of the solid depending on the fluid fraction, is made clear in the revised manuscript. Besides the explanation under the superscript 1) of Table 1, we have added the following sentence at the end of the third paragraph of Section 4 (L253-254): *It is further important to note that  $\delta$  scales linearly with the solid fraction – this means that the values given in Table 1 only apply for 100% solid.*
- “Reasonably good correspondence”: as there are no fixed criteria available to our knowledge what is a good correspondence, this is to some extent based on expert knowledge, summarizing the essence of Table 3. In Table 3, we have now defined the levels of empirical adequacy: empirically adequate = within the documented range of values; empirically partly adequate = less than 50% away from the documented range of values; empirically inadequate = at least 50% away from the documented range of values. The arithmetic means of minimum and maximum of each range are used for the calculation.
- We have added detail maps of the alluvial fan in Fig. 8 and Fig. 11, showing the observed and simulated impact areas.
- The zones were defined according to geomorphologic criteria and dominant process type. We have tried to formulate this in a clearer way in the revised manuscript. The newly introduced Fig. 4 further illustrates these characteristics and process types, in addition to Table 1.

2) Mass balance: in 220 you write that “only heights <0.25 m are taken into account for the visualization and evaluation of the simulation results”. That’s ok for the visualization part but what about mass balance? how much impact do have diffusion effects in your model? how much material you discard when you filter at 0.25 m?

This is an important point. The threshold of 0.25 m does not affect the mass balance, as it is only applied to visualization and evaluation, but not to the simulation itself. However, there is also a minimum flow height considered in the simulation – a value of 0.01 m was chosen in this case. In scenario 2, the volume of the initial landslide decreased from 3.462 million m<sup>3</sup> at release to 3.437 million m<sup>3</sup> at deposition, which is 0.7% and therefore negligible, at least for the purpose of the present study. Indeed, loss of material was an issue in the rather channelized Bondasca Valley, where the flow boundary, where loss of material occurs, is large compared to the flow width and flow area: in scenario 1, almost 12% of the flow material “disappeared” due to numerical diffusion until the flow reached the outlet of Val Bondasca. In the revised manuscript, we have reduced the numerical loss of material by recomputing both scenarios, decreasing the minimum flow height for the simulation from 0.01 to 0.001 m: now, the losses until the outlet is reached are below 1% for the Scenario S1, and below 4% for the Scenario S2 for each phase. This has increased the volumes reaching the outlet of Val Bondasca, but did not change the general

patterns and messages. Figures and numbers were updated accordingly in the revised manuscript, and the following statement was added at L257–259:

*A threshold of 0.001 m is used for the simulation itself, keeping the loss due to numerical diffusion within a range of <1–4% until the point when the flow first leaves the area of interest.*

#### SPECIFIC COMMENTS

I 47-49: as a matter of taste I do not think that putting 14 references after a sentence contributes much to the clarity and readability of a paper and to the whole general usefulness for supporting a scientific discourse (that should be the main reason for inserting citations in an introduction)

The intention of the large number of references put here was to highlight the importance of the topic and to strongly support the statements. However, we can follow the argument of the reviewer and have reduced the number of references to four articles published in the last ten years.

I 88: insert a couple of words to explain how these displacements were monitored

This information was added: mainly radar interferometry, but also laser scanning was applied to measure the displacements.

I 94 and following: check that each acronym has its own definition the first time they appear in the text. Moreover the VAW and WSL reports are written in German so it is not easy to extract the required information. Please if you refer to these works add a sentence summarizing the useful findings.

We have added an introductory paragraph to Section 2.2, where the abbreviations are explained (L101-104):

*“The complex landslide which occurred on 23 August 2017 was documented mainly by reports of the Swiss Federal Institute for Forest, Snow and Landscape Research (WSL), the Laboratory of Hydraulics, Hydrology and Glaciology (VAW) of the ETH Zurich, and the Amt für Wald und Naturgefahren (Office for Forest and Natural Hazards) of the canton of Grisons.”*

Those main points of these sources which are relevant for the present work are mentioned in the text, particularly in the sections 2.2 and 2.3.

I 100-102: insert data about the average steepness of the tract. In fact in the whole paper little information about the local heights and steepness are inferable. In Fig 1 the contour lines labels are missing and in the following maps the contour lines are missing altogether. I would suggest the authors to add the labels in fig. 1 and to insert a table or a figure with the average steepness of the channel profile in each of the 6 zones.

Indeed, this is an important point. In the revised manuscript we provide an additional figure (the new Fig. 4) showing a profile of the path with the elevation and slope information added, and also some information with regard to the individual zones. For this purpose, we have re-analyzed the geometric properties and included some minor updates of travel distances, drop heights, and angles of reach. Further, Fig. 1 has been equipped with contour line labels.

I 109: is it possible to talk about rock avalanche with an angle of reach of 28 and no brandung? refer to Nicoletti 1991, Corominas 1996 and Hungr 2005 and discuss

We follow the revised Varnes classification (Hungr et al., 2014) – there, rock avalanches are essentially described as pieces of rock moving as one mass like a flow, instead of individual blocks. This clearly corresponds to those descriptions of the event in Zone C which are available to us. Nevertheless, we fully agree that the issue of the angle of reach and run-up is very relevant in this context, deserving some further attention. Therefore, we have added the following text (L125-129):

*“This value is higher than the 22° predicted by the equation of Scheidegger (1973), probably due to the sharp deflection of the initial landslide. Following the concept of Nicoletti and Sorriso-Valvo (1991), the rock avalanche was characterized by channelling of the mass. Only a limited run-up was observed, probably due to the gentle horizontal curvature of the valley in that area (no orthogonal impact on the valley slope; Hewitt, 2002).”*

Corominas (1996) and Hungr et al. (2005) do not explicitly consider rock avalanches, but other types of landslides, so in our opinion it would not be appropriate to include these references here.

I 116: did you filtered the errors in the volume estimation? If yes, how?

The volume was calculated comparing the DSM made by photogrammetry and the DEM from the government with a 2 m resolution. Errors might come from the fact that we compare the 2017 DSM with a DEM previous to the 2011 event. The structures on the surface were used to exclude the 2011 volume, a procedure connected to an uncertainty of few 100,000s of cubic metres, when comparing the most plausible boundaries between the release areas of the two events. This may also explain the slight discrepancies between the volumes reported in different sources. Compared to the initial manuscript, we have revised the volume estimate and arrived at 3.2–3.3 million m<sup>3</sup> for the initial rock slide, which corresponds better to other reports than the initial estimate of almost 3.5 million m<sup>3</sup> (see the updated Fig. 5). No further filtering was carried out.

Fig 8 – please put hydrograph a and b to the left

We have rearranged the panes of Fig. 8 accordingly.

## Back-calculation of the 2017 Piz Cengalo-Bondo landslide cascade with r.avaflow

*Martin Mergili, Michel Jaboyedoff, José Pullarelli, Shiva P. Pudasaini*

### Response to the comments of Referee #2 (Brian McArdell)

We would like to thank the reviewer for the constructive remarks. Below, we address each comment in full detail. Our response is written in blue colour. **Changes in the manuscript are highlighted in yellow colour.**

This manuscript describes the application of r.avaflow to a two-process sediment cascade involving a rock avalanche and subsequent debris flows. While the manuscript is interesting, clear and concise and is certainly of interest to users of r.avaflow, the manuscript has the character of a case study and the application of the model and concepts to other field sites is limited by the fact that the model must be calibrated for every new application. This suggests that r.avaflow is perhaps only useful for post-event analysis and not for predictive hazard analyses.

Yes, this is an important point. Indeed, we currently do not recommend r.avaflow for predictive simulations of complex landslides, as the understanding of the parameterization is not good enough. It is exactly this type of study presented here which we consider important to improve this understanding and the related challenges. We have tried to better highlight this key point of the work in the discussion and the conclusions of the revised manuscript. At the beginning of the last paragraph of the discussion, we have therefore added the following sentence (L421-424):

*The present work is seen as a further step towards a better understanding of the challenges and the parameterization concerning the integrated simulation of complex mass flows. More case studies are necessary to derive guiding parameter sets facilitating predictive simulations of such events (Mergili et al., 2018a, b).*

And at the end of the conclusions (L450-451):

*Finally, more case studies of complex mass flows have to be performed in order to derive guiding parameter sets serving for predictive simulations.*

r.avaflow is not the only model capable of describing such coupled processes, but readers may well get this impression after reading the manuscript. At a minimum, a discussion of other models and how they also described similar process transitions would be helpful for the reader, e.g. Iverson et al.'s work on runout modelling of the Oso landslide. The manuscript requires some new literature sections (other models), some new discussion sections (shortcomings and advantages of both models), and a few relatively minor clarifications (below) before it can be published. Some minor points are listed below.

See detailed comments below.

General Comments

1. Is it accurate to call r.avaflow a GIS-based model? Certainly the user interface relies extensively on a GIS interface, but I was under the impression that the model is based on a numerical solution of the shallow-water equations for granular flows, e.g. the flow model written mainly by Shiva Pudasaini.

This is a good point. In our opinion, it is an issue of wording. We would certainly call r.avaflow a GIS-based *tool*, as it strongly relies on GIS data as input, and also provides GIS data as output. The Pudasaini (2012) *model* is not directly GIS-based, we fully agree with that. Therefore, we refer to r.avaflow as a GIS-based *tool* in the revised manuscript, instead of a GIS-based numerical *model*.

2. While it is certainly efficient to refer to previous publications about the model and to not re-state the equations used in the model, I think that some description of the equations solved in the model would be appropriate for the reader. Otherwise, it is impossible to understand the manuscript without referring to the paper where the model is described. Does it include terms to describe the influence of curvature on the solution?

This is, in our opinion, a very controversial issue with this type of case studies. Even though we can follow the thoughts behind the suggestion, the problem is that just showing the main equations would open up more questions than it would answer – covering the equations in sufficient detail would make the paper extremely lengthy and would distract the readers from the actual topic of trying to reproduce the Piz Cengalo-Bondo event and push the work in a direction which differs from the intended one. Therefore, we strongly prefer to refrain from re-describing the fundamental equations behind the tool. The effects of curvature are implicitly reflected in the optimized parameter set, but are not explicitly considered in this specific set of simulations. A comprehensive and proper implementation of curvature terms will be an important aspect in the future (we are already working on it), but is not subject of the present work.

3. Section 5: Please define CSI, D2PC, and FoC. Interested readers should at least be able to see how they are defined without having to refer to the Mergili et al., 2018b paper. This is only a few sentences and it would save interested readers a fair amount of work.

Yes, this is a good point. In the revised manuscript, we have added a brief description of these three parameters at the end of the first paragraph of Section 5 (L269-273):

*CSI and D2PC measure the correspondence of the observed and simulated impact areas. Both indicators can range between 0 and 1, whereby values of CSI close to 1 and values of D2PC close to 0 point to a good correspondence. FoC indicates whether the observed impact areas are overestimated ( $FoC > 1$ ), or underestimated by the simulation ( $FoC < 1$ ). More details are provided by Formetta et al. (2015) and by Mergili et al. (2017, 2018a).*

4. Lines 211, 284, 290,340, and possibly elsewhere: I have no idea what you mean by the term “empirical adequacy” which sounds like it could include anything that is physically possible (instead of physically plausible). Please use a different expression.

*Empirical adequacy* just means that the simulation results are in line with the reference data, telling nothing about physical plausibility. The term was used e.g. by Oreskes et al. (1994) and, in our opinion, describes exactly what we want it to describe. We would not know about a better term for that.

Oreskes, N., Shrader-Frechette, K., & Belitz, K. (1994). Verification, validation, and confirmation of numerical models in the earth sciences. *Science*, 263(5147), 641-646.

5. Lines 284-292: I've heard similar statements by Prof. Florian Amann and I believe it was also mentioned by S. Demmel in her masters thesis, or in the WSL 2017 report. I have seen this idea presented this several times at different conferences, so it is unfair to not at least mention that it is not your hypothesis.

Yes, we have added the reference to Walter et al. (2019) where mentioning the injection of water into the rock avalanche (L343).

6. Others (e.g. Iverson & George) have developed similar two-phase models that are capable of describing process chains. This paper gives a false impression that r.avaflow is the only model capable of describing the runout of coupled processes. Please include a few paragraphs describing and/or comparing and contrasting your model with previous ones.

Yes, we can follow this point of criticism. In the revised manuscript, the model of Iverson and George (2014) and the software D-Claw are mentioned in the introduction, and also in the Discussion. However, in our opinion this approach shows various shortcomings, compared to the Pudasaini (2012) model: Iverson and George (2014) presented a depth-averaged two-phase mass flow model which includes five field variables: the evolution of the solid volume fraction, basal pore-fluid pressure, flow thickness and the bulk velocities. The source terms account for the influence of the granular dilation rate. The model is based on several postulates and empirical relations, including the dilation rate. However, the model assumes that the solid and fluid velocities are the same. Instead of naturally occurring six field variables, in their model, there are only five field variables. So, from the general two-phase perspective, their system is not complete, as in general, the relative velocity between the solid and fluid phase is not negligible. Moreover, their pore fluid pressure evolution equation only includes pore pressure advection and some source terms associated with dilation, but ignores the pore fluid diffusion, another potentially important aspect of fluid flow dynamics in mixture mass flows (Iverson and Denlinger, 2001; Pudasaini et al., 2005). There are no real interfacial momentum transfers, such as the drag force, virtual mass force and buoyancy between the solid and fluid phases. Furthermore, as the fluid pressure evolution is assumed to play a substantial role in their debris flow model, then the solid and fluid dynamics cannot be similar, and thus assumption of negligible relative velocity between solid and fluid is questionable (Pitman and Le, 2005; Pudasaini, 2012). Iverson and George (2014) do not consider viscous shear stress, which can play crucial role in the natural debris flows (Pitman and Le, 2005; Takahashi, 2007; Pudasaini, 2012). Moreover, in situations when the solid material behaves as isotropic material, in Iverson and George (2014) there is no dynamical coupling between the pore fluid pressure evolution and the bulk momentum equations, interactions appear only via source terms that also disappear in liquefaction.

As discussed, the Pudasaini (2012) model is the most general two-phase mass flow model that exists today, that includes all the basic mechanics and flow dynamical aspects of real two-phase solid fluid



mixture mass flows with strong interfacial momentum transfer between the phases. The model can be used for any mixture composition of solid and fluid, including dry and fluid limits. So, it has been successfully applied to different flow scenarios including the cascading natural events (Mergili et al., 2017, 2018a, 2018b).

Although the Iverson and George (2014) model is restricted from the real phase-interactions, this model could still be useful for very dense debris flows where the solid particles and fluid molecules move together. The model has been solved with in an open source software, called D-Claw (George and Iverson, 2014). And the model output has been compared with some results from two sets of large-scale experiments of debris flow mobilization (Iverson RM, Reid ME, Iverson NR, LaHusen RG, Logan M, Mann JE, Brien DL 2000 Acute sensitivity of landslide rates to initial soil porosity. *Science* 290, 513-516. (doi:10.1126/science.290.5491.513)), and debris-flow dynamics and deposition (Iverson RM, Logan M, LaHusen RG, Berti M 2010 The perfect debris flow? aggregated results from 28 large-scale experiments. *J. Geophys. Res.* 115, 1-29. (doi:10.1029/2009JF001514)), both with dense debris materials.

Since there are no explicit and independent equations for the solid and fluid phase momentum transfer the model by Iverson and George (2014) cannot be applied for cascading mass flows, such as landslides impacting fluid reservoirs (Pudasaini, 2014; Kafle et al., 2016, 2019), or glacial lake outburst floods (Kattel et al., 2016).

Consequently, the model of Iverson and George (2014) is mentioned in the introduction of the revised manuscript, and the following statement (mostly summarizing what was said above) has been added to the discussion (L357-372):

*Still, we currently consider the Pudasaini (2012) model – and the extended multi-phase model (Pudasaini and Mergili, 2019) – best practice, even though other two-phase or bulk mixture models do exist. Most recently, Iverson and George (2014) presented an approach that has been solved with an open source software, called D-Claw (George and Iverson, 2014), and compared to large-scale experiments considering dense debris materials (Iverson et al., 2000; Iverson et al., 2010). The Iverson and George (2014) model can be useful for very dense debris flows where the solid particles and fluid molecules move together. However, its applicability to cascading mass flows is limited for the following reasons: (i) this model assumes that the solid and fluid velocities are the same, an assumption that does not hold for complex, cascading mass flows; (ii) the pore fluid pressure evolution equation includes pore pressure advection and source terms associated with dilation, but ignores the pore fluid diffusion; (iii) there are no real interfacial momentum transfers, such as the drag force, virtual mass force, and buoyancy between the solid and fluid phases; and (iv) neither viscous shear stress, nor dynamical coupling between the pore fluid pressure evolution and the bulk momentum equations are considered. Furthermore, as the fluid pressure evolution is assumed to play a substantial role in the Iverson and George (2014) model, the solid and fluid dynamics cannot be similar, and thus the assumption of negligible relative velocity between solid and fluid is questionable (Pitman and Le, 2005; Pudasaini, 2012).*

#### Specific comments

Lines 85-86: The statement that the deposit did not connect to the main channel of Val Bondasca is incorrect. The 2011 deposit certainly covered the uppermost part of the Val Bondasca and therefore is

connected hydrologically and geomorphologically. The main torrent channel after the 2011 event went over and eroded the deposits of the 2011 rock avalanche deposit. Please correct this error, or more precisely state how it was “not connected”. This is clearly evident in publications of others, e.g. Frank et al. (2019) which illustrates the triggering of debris flows in Val Bondasca following the 2011 rock avalanche. Frank, F., Huggel, C., McArdell, B. W., & Vieli, A.(2019). Landslides and increased debris-flow activity: a systematic comparison of six catchments in Switzerland. *Earth Surface Processes and Landforms*, 44(3), 699-712.<https://doi.org/10.1002/esp.4524>.

Thanks a lot for this comment and the reference. We have changed the text accordingly (L89-93):

*On 27 December 2011, a rock avalanche with a volume of 1.5–2 million m<sup>3</sup> developed out of a rock toppling from the NE face of Piz Cengalo, travelling for a distance of 1.5 km down to the uppermost part of the Val Bondasca (Haeberli et al., 2013; De Blasio and Crosta, 2016; Amann et al., 2018). This rock avalanche reached the main torrent channel. Erosion of the deposit thereafter resulted in increased debris flow activity (Frank et al., 2019).*

Lines 102-103. These data are almost certainly from the Canton of Grisons and not from the WSL, although they were certainly repeated in the WSL 2017 report.

We only found the data in the WSL report and have completed the reference as follows:

*data from the Canton of Grisons reported by WSL, 2017*

Lines 129-130. This statement about the pore-water pressure rise is somewhat speculative and should be treated as a hypothesis and not as a fact. Rock avalanche deposits (e.g. the 2011 deposits) are often described as having relatively low porosity, and therefore one could, possibly, also expect dilation upon compression which would cause a drop in pore-water pressure and not a rise. The river-bed sediments, and possibly the moraine deposits, upon which the 2017 rock avalanche flowed would be more reasonable candidates for the mechanism you describe here.

We absolutely agree that the pore water pressure rise is a hypothesis rather than a fact. This is also clearly indicated by the start of the sentence: *Walter et al. (2019) claim that ...*

Lines 221-222: Did you try other grid resolutions? This resolution, based on my own experience using CFD models (also with a GIS user interface) indicates to me that the grid size is fine for the rock avalanche runout modelling but too coarse for the debris-flow runout modelling.

This is an important issue, indeed. We have also tried 5 m resolution, but the results for this specific case were not substantially different, only the computational time increased considerably.

Line 237: What do you mean by total discharge? The sum of the discharge of all of the phases, or the sum of different flow paths comprising the flow. Or do you mean maximum discharge or the maximum discharge sum of all of the phases? From the text it appears to be a peak discharge value and not just a total value.

With total discharge, we meant solid+fluid discharge. The text was reformulated accordingly in order to avoid confusion.

Line 346: A brief re-statement of the Scenarios would be reasonable here for the reader.

We have reformulated the start of the conclusions as follows (L436-437):

*Both of the investigated Scenarios S1 (debris flow developing at the front of the rock avalanche) and S2 (debris flow developing at the back of the rock avalanche, overtopping the deposit) ...*

Table 1: It's confusing to have Zones A, B, and so on, as well as scenario sets A & B. perhaps you could use lower-case letters for scenarios a and b, or use something like SA or SB to make it completely unambiguous.

Yes, this is true – we have changed the names of the scenarios to S1 and S2.

Figure 5 is a nice graphical depiction of the two scenarios.

Thank You!

# 1 **Back-calculation of the 2017 Piz Cengalo-Bondo landslide cas-** 2 **cade with r.avaflow**

3 ***Martin Mergili*<sup>1,2</sup>, *Michel Jaboyedoff*<sup>3</sup>, *José Pullarello*<sup>3</sup>, *Shiva P. Pudasaini*<sup>4</sup>**

4 <sup>1</sup> Institute of Applied Geology, University of Natural Resources and Life Sciences (BOKU), Peter-Jordan-  
5 Straße 82, 1190 Vienna, Austria

6 <sup>2</sup> Geomorphological Systems and Risk Research, Department of Geography and Regional Research, Uni-  
7 versity of Vienna, Universitätsstraße 7, 1010 Vienna, Austria

8 <sup>3</sup>Institute of Earth Sciences, University of Lausanne, Quartier UNIL-Mouline, Bâtiment Géopolis, 1015  
9 Lausanne, Switzerland

10 <sup>4</sup> Institute of **Geosciences**, Geophysics Section, University of Bonn, Meckenheimer Allee 176, 53115  
11 Bonn, Germany

12 Correspondence to: M. Mergili (martin.mergili@boku.ac.at)

## 13 **Abstract**

14 In the morning of 23 August 2017, around 3 million m<sup>3</sup> of granitoid rock broke off from the east face of  
15 Piz Cengalo, SE Switzerland. The initial rock slide-rock fall entrained 0.6 million m<sup>3</sup> of a glacier and  
16 continued as a rock(-ice) avalanche, before evolving into a channelized debris flow that reached the  
17 village of Bondo at a distance of 6.5 km after a couple of minutes. Subsequent debris flow surges fol-  
18 lowed in the next hours and days. The event resulted in eight fatalities along its path and severely dam-  
19 aged Bondo. The most likely candidates for the water causing the transformation of the rock avalanche  
20 into a long-runout debris flow are the entrained glacier ice and water originating from the debris be-  
21 neath the rock avalanche. In the present work we try to reconstruct conceptually and numerically the  
22 cascade from the initial rock slide-rock fall to the first debris flow surge and thereby consider two sce-  
23 narios in terms of qualitative conceptual process models: (i) entrainment of most of the glacier ice by the  
24 frontal part of the initial rock slide-rock fall and/or injection of water from the basal sediments due to  
25 sudden rise in pore pressure, leading to a frontal debris flow, with the rear part largely remaining dry  
26 and depositing mid-valley; and (ii) most of the entrained glacier ice remaining beneath/behind the  
27 frontal rock avalanche, and developing into an avalanching flow of ice and water, part of which overtops  
28 and partially entrains the rock avalanche deposit, resulting in a debris flow. Both scenarios can **– with**  
29 **some limitations –** be numerically reproduced with the two-phase mass flow model **(Pudasaini, 2012)**  
30 implemented with the simulation software r.avaflow, based on plausible assumptions of the model pa-  
31 rameters. However, these simulation results do not allow to conclude on which of the two scenarios is  
32 the more likely one. Future work will be directed towards the application of a three-phase flow model

33 (rock, ice, fluid) including phase transitions, in order to better represent the melting of glacier ice, and a  
34 more appropriate consideration of deposition of debris flow material along the channel.

35 Keywords: Debris flow, Entrainment, High-mountain process chain, Rock avalanche, Two-phase flow  
36 model, r.avaflow

## 37 **1 Introduction**

38 Landslides lead to substantial damages to life, property, and infrastructures every year. Whereas initial  
39 landslides in hilly terrain have mostly local effects, landslides in high-mountain areas, with elevation  
40 differences of thousands of metres over a few kilometres may form the initial points of process chains  
41 which, due to their interactions with glacier ice, snow, lakes, or basal material, sometimes evolve into  
42 long-runout debris avalanches, debris flows or floods. Such complex landslide events may occur in re-  
43 mote areas, such as the 2012 Alpl rock-snow avalanche in Austria (Preh and Sausgruber, 2015) or the  
44 2012 Santa Cruz multi-lake outburst event in Peru (Mergili et al., 2018a). If they reach inhabited areas,  
45 such events lead to major destruction even several kilometres away from the source and have led to ma-  
46 jor disasters in the past, such as the 1949 Khait rock avalanche-loess flow in Tajikistan (Evans et al.,  
47 2009b); the 1962 and 1970 Huascarán rock fall-debris avalanche events in Peru (Evans et al., 2009a;  
48 Mergili et al., 2018b); the 2002 Kolka-Karmadon ice-rock avalanche in Russia (Huggel et al., 2005); the  
49 2012 Seti River debris flood in Nepal (Bhandari et al., 2012); or the 2017 Piz Cengalo-Bondo rock ava-  
50 lanche-debris flow event in Switzerland. The initial fall or slide sequences of such process chains are  
51 commonly related to a changing cryosphere such as glacial debuttressing, the formation of hanging glac-  
52 iers, or a changing permafrost regime (Harris et al., 2009; Krautblatter et al., 2013; Haeberli and  
53 Whiteman, 2014; Haeberli et al., 2017).

54 Computer models assist risk managers in anticipating the impact areas, energies, and travel times of  
55 complex mass flows. Conventional single-phase flow models, considering a mixture of solid and fluid  
56 components (e.g. Voellmy, 1955; Savage and Hutter, 1989; Iverson, 1997; McDougall and Hungr, 2004;  
57 Christen et al., 2010), do not serve for such a purpose. Instead, simulations rely on (i) model cascades,  
58 changing from one approach to the next at each process boundary (Schneider et al., 2014; Somo-  
59 Valenzuela et al., 2016); or (ii) bulk mixture models or two- or even multi-phase flow models (Pit-  
60 man and Le, 2005; Pudasaini, 2012; Iverson and George, 2014; Mergili et al., 2017). Worni et al. (2014)  
61 have highlighted the advantages of (ii) for considering also the process interactions and boundaries.  
62 Two- or multi-phase flow models separately consider the solid and the fluid phase, but also phase inter-  
63 actions.

64 The aim of the present work is to learn about our ability to reproduce sophisticated transformation  
65 mechanisms involved in complex, cascading landslide processes, with GIS-based tools. For this purpose,  
66 we apply the computational tool r.avaflow (Mergili et al., 2017), which employs an enhanced version of  
67 the Pudasaini (2012) two-phase flow model, to back-calculate the 2017 Piz Cengalo-Bondo landslide  
68 cascade in SE Switzerland, which was characterized by the transformation of a rock avalanche to a long-  
69 runout debris flow. We consider two scenarios in terms of hypothetical qualitative conceptual models of  
70 the physical transformation mechanisms. On this basis, we try to numerically reproduce these scenarios,  
71 satisfying the requirements of physical plausibility of the model parameters, and empirical adequacy in  
72 terms of correspondence of the results with the documented and inferred impact areas, volumes, veloci-  
73 ties, and travel times. Based on the outcomes, we identify the key challenges to be addressed in future  
74 research.

75 Thereby we rely on the detailed description, documentation, and topographic reconstruction of this  
76 recent event. The event documentation, data used, and the conceptual models are outlined in Section 2.  
77 We briefly introduce the simulation framework r.avaflow (Section 3) and explain its parametrization  
78 and our simulation strategy (Section 4) before presenting (Section 5) and discussing (Section 6) the re-  
79 sults obtained. Finally, we conclude with the key messages of the study (Section 7).

## 80 **2 The 2017 Piz Cengalo-Bondo landslide cascade**

### 81 **2.1 Piz Cengalo and Val Bondasca**

82 The Val Bondasca is a left tributary valley to the Val Bregaglia in the canton of the Grisons in SE Swit-  
83 zerland (Fig. 1). The Bondasca stream joins the Mera River at the village of Bondo at 823 m asl. It drains  
84 part of the Bregaglia Range, built up by a mainly granitic intrusive body culminating at 3678 m asl. Piz  
85 Cengalo, with a summit elevation of 3368 m asl, is characterized by a steep, intensely fractured NE face  
86 which has repeatedly been the scene of landslides, and which is geomorphologically connected to the  
87 Val Bondasca through a steep glacier forefield. The glacier itself has largely retreated to the cirque be-  
88 neath the rock wall.

89 On 27 December 2011, a rock avalanche with a volume of 1.5–2 million m<sup>3</sup> developed out of a rock top-  
90 pling from the NE face of Piz Cengalo, travelling for a distance of 1.5 km down to the uppermost part of  
91 the Val Bondasca (Haeberli et al., 2013; De Blasio and Crosta, 2016; Amann et al., 2018). This rock ava-  
92 lanche reached the main torrent channel. Erosion of the deposit thereafter resulted in increased debris  
93 flow activity (Frank et al., 2019). No entrainment of glacier ice was documented for this event. As blue  
94 ice had been observed directly at the scarp, the role of permafrost for the rock instability was discussed.

95 An early warning system was installed and later extended (Steinacher et al., 2018). Displacements at the  
96 scarp area, measured by radar interferometry and laser scanning, were few centimetres per year between  
97 2012 and 2015, and accelerated in the following years. In early August 2017, increased rock fall activity  
98 and deformation rates alerted the authorities. A major rock fall event occurred on 21 August 2017  
99 (Amann et al., 2018).

## 100 2.2 The event of 23 August 2017

101 The complex landslide which occurred on 23 August 2017 was documented mainly by reports of the  
102 Swiss Federal Institute for Forest, Snow and Landscape Research (WSL), the Laboratory of Hydraulics,  
103 Hydrology and Glaciology (VAW) of the ETH Zurich, and the Amt für Wald und Naturgefahren (Office  
104 for Forest and Natural Hazards) of the canton of Grisons.

105 At 9:31 am local time, a volume of approx. 3 million m<sup>3</sup> detached from the NE face of Piz Cengalo, as  
106 indicated by WSL (2017); Amann et al. (2018); and the point cloud we obtained through structure from  
107 motion using pictures taken after the event. Documented by videos and by seismic records (Walter et al.,  
108 2018), it impacted the glacier beneath the rock face and entrained approx. 0.6 million m<sup>3</sup> of ice (VAW,  
109 2017; WSL, 2017), was sharply deflected at an opposite rock wall, and evolved into a rock(-ice) ava-  
110 lanche. Part of this avalanche immediately converted into a debris flow which flowed down the Val  
111 Bondasca. It was detected at 9:34 by the debris flow warning system which had been installed near the  
112 hamlet of Prä approx. 1 km upstream from Bondo. According to different sources, the debris flow surge  
113 arrived at Bondo between 9:42 (derived from WSL, 2017) and 9:48 (Amt für Wald und Naturgefahren,  
114 2017). The rather low velocity in the lower portion of the Val Bondasca is most likely a consequence of  
115 the narrow gorge topography, and of the viscous behaviour of this first surge. Whereas approx.  
116 540,000 m<sup>3</sup> of material were involved, only 50,000 m<sup>3</sup> arrived at Bondo immediately (data from the Can-  
117 ton of Grisons reported by WSL, 2017). The remaining material was partly remobilized by six further  
118 debris flow surges recorded during the same day, one on 25 August, and one – triggered by rainfall – on  
119 31 August 2017. All nine surges together deposited a volume of approx. 500,000–800,000 m<sup>3</sup> in the area  
120 of Bondo, less than half of which was captured by a retention basin (Bonanomi and Keiser, 2017).

121 The vertical profile of the main flow path is illustrated in Fig. 4. The total angle of reach of the process  
122 chain from the initial release down to the outlet of the Bondasca Valley was approx. 17.4°, computed  
123 from the travel distance of 7.0 km and the vertical drop of approx. 2.2 km. The initial landslide to the  
124 terminus of the rock avalanche showed an angle of reach of approx. 25.8°, derived from the travel dis-  
125 tance of 3.4 km and the vertical drop of 1.7 km. This value is higher than the 22° predicted by the equa-  
126 tion of Scheidegger (1973), probably due to the sharp deflection of the initial landslide. Following the

127 concept of Nicoletti and Sorriso-Valvo (1991), the rock avalanche was characterized by channelling of  
128 the mass. Only a limited run-up was observed, probably due to the gentle horizontal curvature of the  
129 valley in that area (no orthogonal impact on the valley slope; Hewitt, 2002). There were eight fatalities,  
130 concerning hikers in the Val Bondasca, extensive damages to buildings and infrastructures, and evacua-  
131 tions for several weeks or even months.

### 132 2.3 Data and conceptual model

133 Reconstruction of the rock and glacier volumes involved in the event was based on an overlay of a 2011  
134 swisstopo MNS-Digital Elevation Model (DEM) (contract: swisstopo–DV084371), derived through air-  
135 borne laser scanning in 2011 and available at a raster cell size of 2 m, and a Digital Surface Model (DSM)  
136 obtained through Structure from Motion (SfM) techniques after the 2017 event. This analysis resulted in  
137 a detached rock volume of 3.27 million m<sup>3</sup>, which is slightly more than the value of 3.15 million m<sup>3</sup>  
138 reported by Amann et al. (2018), and an entrained ice volume of 770,000 m<sup>3</sup> (Fig. 5). However, these  
139 volumes neglect smaller rock falls before and after the large 2017 event, and also glacial retreat. The  
140 2011 event took place after the DTM had been acquired, but it released from an area above the 2017  
141 scarp. The boundary between the 2011 and the 2017 scarps, however, is slightly uncertain, which ex-  
142 plains the discrepancies between the different volume reconstructions. Assuming some minor entrain-  
143 ment of the glacier ice in 2011 and some glacial retreat, we arrive at an entrained ice volume of  
144 600,000 m<sup>3</sup>, a value which is very well supported by VAW (2017).

145 There is still disagreement on the origin of the water having led to the debris flow, particularly to the  
146 first surge. Bonanomi and Keiser (2017) clearly mention meltwater from the entrained glacier ice as the  
147 main source, whereby much of the melting is assigned to impact, shearing and frictional heating directly  
148 at or after impact, as it is often the situation in rock-ice avalanches (Pudasaini and Krautblatter, 2014).  
149 WSL (2017) has shown, however, that the energy released was only sufficient to melt approx. half of the  
150 glacier ice. Water pockets in the glacier or a stationary water source along the path might have played  
151 an important role (Demmel, 2019). Walter et al. (2019) claim that much of the glacier ice was crushed,  
152 ejected and dispersed (Fig. 3b), whereas water injected into the rock avalanche due to pore pressure rise  
153 in the basal sediments would have played a major role. In any case, the development of a debris flow  
154 from a landslide mass with an overall solid fraction of as high as ~0.85 (considering the water equivalent  
155 of the glacier ice) requires some spatio-temporal differentiation of the water/ice content. We consider  
156 two qualitative conceptual models – or scenarios – possibly explaining such a differentiation:

157 S1 The initial rock slide-rock fall led to massive entrainment, fragmenting and melting of glacier  
158 ice, mixing of rock with some of the entrained ice and the meltwater, and injection of water



159 from the basal sediments into the rock avalanche mass quickly upon impact due to overload-  
160 induced pore pressure rise. As a consequence, the front of the rock avalanche was characterized  
161 by a high content of ice and water, highly mobile, and therefore escaped as the first debris flow  
162 surge, whereas the less mobile rock avalanche behind – still with some water and ice in it – de-  
163 celerated and deposited mid-valley. The secondary debris flow surges occurred mainly due to  
164 backwater effects. This scenario largely follows the explanation of Walter et al. (2019) that the  
165 first debris flow surge was triggered at the front of the rock avalanche by overload and pore  
166 pressure rise, whereas the later surges overtopped the rock avalanche deposits, as indicated by  
167 the surficial scour patterns.

168 S2 The initial rock slide-rock fall impacted and entrained the glacier. Most of the entrained ice re-  
169 mained beneath and developed into an avalanching flow of melting ice behind the rock ava-  
170 lanche. The rock avalanche decelerated and stopped mid-valley. Part of the avalanching flow  
171 overtopped and partly entrained the rock avalanche deposit – leaving behind the scour traces ob-  
172 served in the field – and evolved into the channelized debris flow which arrived at Bondo a cou-  
173 ple of minutes later. The secondary debris flow surges started from the rock avalanche deposit  
174 due to melting and infiltration of the remaining ice, and due to backwater effects. This scenario  
175 is similar to the theory developed at the WSL Institute for Snow and Avalanche Research (SLF),  
176 who also did a first simulation of the rock avalanche (WSL, 2017).

177 Fig. 6 illustrates the conceptual models attempting to explain the key mechanisms involved in the rock  
178 avalanche-debris flow transformation.

### 179 **3 The simulation framework r.avaflow**

180 r.avaflow represents a comprehensive GIS-based open source framework which can be applied for the  
181 simulation of various types of geomorphic mass flows. In contrast to most other mass flow simulation  
182 tools, r.avaflow utilizes a general two-phase-flow model describing the dynamics of the mixture of solid  
183 particles and viscous fluid and the strong interactions between these phases. It further considers erosion  
184 and entrainment of surface material along the flow path. These features facilitate the simulation of cas-  
185 cading landslide processes such as the 2017 Piz Cengalo-Bondo event. r.avaflow is outlined in full detail  
186 by Mergili and Pudasaini (2019). The code, a user manual, and a collection of test datasets are available  
187 from Mergili (2019). Only those aspects directly relevant for the present work are described in this sec-  
188 tion.

189 Essentially, the Pudasaini (2012) two-phase flow model is employed for computing the dynamics of mass  
 190 flows moving from a defined release area (solid and/or fluid heights are assigned to each raster cell) or  
 191 release hydrograph (at each time step, solid and/or fluid heights are added at a given profile, moving at a  
 192 given cross-profile velocity) down through a DEM. The spatio-temporal evolution of the flow is approx-  
 193 imated through depth-averaged solid and fluid mass and momentum balance equations (Pudasaini,  
 194 2012). This system of equations is solved through the TVD-NOC Scheme introduced by Nessyahu and  
 195 Tadmor (1990), adapting an approach presented by Tai et al. (2002) and Wang et al. (2004). The charac-  
 196 teristics of the simulated flow are governed by a set of flow parameters (some of them are shown in the  
 197 Tables 1 and 2). Compared to the Pudasaini (2012) model, some extensions have been introduced which  
 198 include (i) ambient drag or air resistance (Kattel et al., 2016; Mergili et al., 2017); and (ii) fluid friction,  
 199 governing the influence of basal surface roughness on the fluid momentum (Mergili et al., 2018b). Both  
 200 extensions rely on empirical coefficients,  $C_{AD}$  for the ambient drag and  $C_{FF}$  for the fluid friction. Further,  
 201 drag and viscosity are computed according to enhanced concepts. As in Domnik et al. (2013) and Puda-  
 202 saini and Mergili (2019), the fluid viscosity is enhanced by the yield strength. Most importantly, the  
 203 internal friction angle  $\varphi$  and the basal friction angle  $\delta$  of the solid are scaled with the solid fraction in  
 204 order to approximate effects of reduced interaction between the solid particles and the basal surface in  
 205 fluid-rich flows.

206 Entrainment is calculated through an empirical model. In contrast to Mergili et al. (2017), where an em-  
 207 pirical entrainment coefficient is multiplied with the momentum of the flow, here we multiply the en-  
 208 trainment coefficient  $C_E$  ( $\text{s kg}^{-1} \text{m}^{-1}$ ) with the kinetic energy of the flow:

$$209 \quad q_{E,s} = C_E |T_s + T_f| \alpha_{s,E}, \quad q_{E,f} = C_E |T_s + T_f| (1 - \alpha_{s,E}), \quad (1)$$

210 where  $q_{E,s}$  and  $q_{E,f}$  ( $\text{m s}^{-1}$ ) are the solid and fluid entrainment rates,  $T_s$  and  $T_f$  (J) are the kinetic energies of  
 211 the solid and fluid fractions of the flow, and  $\alpha_{s,E}$  is the solid fraction of the entrainable material. Solid  
 212 and fluid flow heights and momenta, and the change of the basal topography, are updated at each time  
 213 step (see Mergili et al., 2017 for details).

214 As r.avaflow operates on the basis of GIS raster cells, its output essentially consists of raster maps –for all  
 215 time steps and for the overall maximum – of solid and fluid flow heights, velocities, pressures, kinetic  
 216 energies, and entrained heights. In addition, output hydrograph profiles may be defined at which solid  
 217 and fluid heights, velocities, and discharges are provided at each time step.

## 218 4 Parameterization of r.avaflow

219 One set of simulations is performed for each of the Scenarios S1 and S2 (Fig. 6), considering the process  
220 chain from the release of the rock slide-rock fall to the arrival of the first debris flow surge at Bondo.  
221 Neither triggering of the event nor subsequent surges or distal debris floods beyond Bondo are consid-  
222 ered in this study. Equally, the dust cloud associated to the rock avalanche (WSL, 2017) is not the subject  
223 here. Initial sliding of the glacier beneath the rock avalanche, as assumed in Scenario S2, cannot directly  
224 be modelled. That would require a three-phase model, which is beyond the scope here. Instead, release  
225 of the glacier ice and meltwater is assumed in a separate simulation after the rock avalanche has passed  
226 over it. We consider this workaround an acceptable approximation of the postulated scenario (Sec-  
227 tion 6).

228 We use the 2011 swisstopo MNS-DEM, corrected for the rock slide-rock fall scarp and the entrained  
229 glacier ice by overlay with the 2017 SfM DSM (Section 2). The maps of release height and maximum  
230 entrainable height are derived from the difference between the 2011 swisstopo DTM and the 2017 SfM  
231 DSM (Fig. 5; Section 2). The release mass is considered completely solid, whereas the entrained glacier is  
232 assumed to contain some solid fraction (coarse till). The glacier ice is assumed to melt immediately on  
233 impact and is included in the fluid along with fine till. We note that the fluid phase does not represent  
234 pure water, but a mixture of water and fine particles (Table 2). The fraction of the glacier allowed to be  
235 incorporated in the process chain is empirically optimized (Table 3). Based on the same principle, the  
236 maximum depth of entrainment of fluid due to pore pressure overload in Scenario S1 is set to 25 cm,  
237 whereas the maximum depth of entrainment of the rock avalanche deposit in Scenario S2 is set to 1 m.

238 The study area is divided into six zones A–F (Fig. 4 and Fig. 7; Table 1). Each of these zones represents  
239 an area with particular geomorphic characteristics and dominant process types, which can be translated  
240 into model parameters. Due to the impossibility to directly measure the key parameters in the field  
241 (Mergili et al., 2018a, b), the parameters summarized in Table 1 and Table 2 are the result of an iterative  
242 optimization procedure, where multiple simulations with different parameter sets are performed in or-  
243 der to arrive at one “optimum” simulation for each scenario. It is thereby important to note that we  
244 largely derive one single set of optimized parameters, which is valid for both of the scenarios. Optimiza-  
245 tion criteria are (i) the empirical adequacy of the model results, and (ii) the physical plausibility of the  
246 parameters. Thereby, the empirical adequacy is quantified through comparison of the results with the  
247 documented impact area, the travel times to the output hydrograph profiles O2, O3, and O4 (Fig. 7), and  
248 the reported volumes (Amt für Wald und Naturgefahren, 2017; Bonanomi and Keiser, 2017; WSL, 2017).  
249 The physical plausibility of the model parameters is evaluated on the basis on the parameters suggested

250 by Mergili et al. (2017) and on the findings of Mergili et al. (2018a, b). The values of the basal friction  
251 angle ( $\delta$ ), the ambient drag coefficient ( $C_{AD}$ ), the fluid friction coefficient ( $C_{FF}$ ), and the entrainment  
252 coefficient ( $C_E$ ) are differentiated between and within the zones (Table 1), whereas global values are  
253 defined for all the other parameters (Table 2). It is further important to note that  $\delta$  scales linearly with  
254 the solid fraction – this means that the values given in Table 1 only apply for 100% solid.

255 Durations of  $t = 1800$  s are considered for both scenarios. At this point of time, the first debris flow surge  
256 has largely passed and left the area of interest, except for some remaining tail of fluid material. Only  
257 heights  $\geq 0.25$  m are taken into account for the visualization and evaluation of the simulation results. A  
258 threshold of 0.001 m is used for the simulation itself, keeping the loss due to numerical diffusion within  
259 a range of  $<1$ – $4\%$  until the point when the flow first leaves the area of interest. Considering the size of  
260 the event, a cell size of 10 m is considered the best compromise between capturing a sufficient level of  
261 detail and ensuring an adequate computational efficiency, and is therefore applied for all simulations.

## 262 5 Simulation results

### 263 5.1 Scenario S1 – Frontal debris flow surge

264 Fig. 8 illustrates the distribution of the simulated maximum flow heights, maximum entrained heights,  
265 and deposition area after  $t = 1800$  s, when most of the initial debris flow surge has passed the confluence  
266 of the Bondasca stream and the Maira river. The comparison of observed and simulated impact areas  
267 results in a critical success index  $CSI = 0.558$ , a distance to perfect classification  $D2PC = 0.167$ , and a fac-  
268 tor of conservativeness  $FoC = 1.455$ . These performance indicators are derived from the confusion matrix  
269 of true positives, true negatives, false positives, and false negatives.  $CSI$  and  $D2PC$  measure the corre-  
270 spondence of the observed and simulated impact areas. Both indicators can range between 0 and 1,  
271 whereby values of  $CSI$  close to 1 and values of  $D2PC$  close to 0 point to a good correspondence.  $FoC$  in-  
272 dicates whether the observed impact areas are overestimated ( $FoC > 1$ ), or underestimated by the simu-  
273 lation ( $FoC < 1$ ). More details are provided by Formetta et al. (2015) and by Mergili et al. (2017, 2018a).

274 Interpreting these values as indicators for a reasonably good correspondence between simulation and  
275 observation in terms of impact area, we now consider the dimension of time, focussing on the output  
276 hydrographs OH1–OH4 (Fig. 9; see Fig. 7 and Fig. 8 for the location of the corresponding hydrograph  
277 profiles O1–O4). Much of the rock avalanche passes the profile O1 between  $t = 60$  s and  $t = 100$  s. OH2  
278 (Fig. 9a; located in the upper portion of Val Bondasca) sets on before  $t = 140$  s and quickly reaches its  
279 peak, with a volumetric solid ratio of approx. 30% (maximum 900 m<sup>3</sup>/s of solid and 2,200 m<sup>3</sup>/s of fluid  
280 discharge). Thereafter, this first surge quickly tails off. The solid flow height, however, increases to

281 around 3 m and remains so until the end of the simulation, whereas the fluid flow height slowly and  
282 steadily tails off. Until  $t = 1800$  s the profile O2 is passed by a total of 221,000 m<sup>3</sup> of solid and 308,000 m<sup>3</sup>  
283 of fluid material (the fluid representing a mixture of fine mud and water with a density of 1,400 kg m<sup>-3</sup>;  
284 see Table 2). The hydrograph profile O3 in Prä, approx. 1 km upstream of Bondo, is characterized by a  
285 surge starting before  $t = 280$  s and slowly tailing off afterwards. Discharge at the hydrograph OH4  
286 (Fig. 9b; O4 is located at the outlet of the canyon to the debris fan of Bondo) starts at around  $t = 700$  s  
287 and reaches its peak of solid discharge at  $t = 1020$  s (167 m<sup>3</sup>/s). Solid discharge decreases thereafter,  
288 whereas the flow becomes fluid-dominated with a fluid peak of 202 m<sup>3</sup>/s at  $t = 1320$  s. The maximum  
289 total flow height simulated at O4 is 2.53 m. This site is passed by a total of 91,000 m<sup>3</sup> of solid and  
290 175,000 m<sup>3</sup> of fluid material, according to the simulation – an overestimate, compared to the documenta-  
291 tion (Table 3).

292 Fig. 10 illustrates the travel time and the frontal velocities of the rock avalanche and the initial debris  
293 flow. The initial surge reaches the hydrograph profile O3 – located 1 km upstream of Bondo – at  
294  $t = 280$  s (Fig. 10a; Fig. 9c). This is in line with the documented arrival of the surge at the nearby moni-  
295 toring station (Table 3). Also the simulated travel time to the profile O4 corresponds to the – though  
296 uncertain – documentation. The initial rock avalanche is characterized by frontal velocities >25 m/s,  
297 whereas the debris flow largely moves at 10–25 m/s. Velocities drop below 5 m/s in the lower part of the  
298 valley (Zone E) (Fig. 10b).

## 299 5.2 Scenario S2 – Debris flow surge by overtopping and entrainment of rock avalanche

300 Fig. 11 illustrates the distribution of the simulated maximum flow heights, maximum entrained heights,  
301 and deposition area after  $t = t_0 + 1740$  s, where  $t_0$  is the time between the release of the initial rock ava-  
302 lanche and the mobilization of the entrained glacier. The simulated impact and deposition areas of the  
303 initial rock avalanche are also shown in Fig. 11. However, we now concentrate to the debris flow, trig-  
304 gered by the entrainment of 145,000 m<sup>3</sup> of solid material from the rock avalanche deposit. Flow heights  
305 – as well as the hydrographs presented in Fig. 9c and d and the temporal patterns illustrated in Fig. 12 –  
306 only refer to the debris flow developing from the entrained glacier and the entrained rock avalanche  
307 material. The confusion matrix of observed and simulated impact areas reveals partly different patterns  
308 of performance than for the Scenario S1:  $CSI = 0.590$ ;  $D2PC = 0.289$ ; and  $FoC = 0.925$ . The lower  $FoC$   
309 value and the lower performance in terms of  $D2PC$  reflect the missing initial rock avalanche in the  
310 simulation results. The output hydrographs OH2 and OH4 differ from the hydrographs obtained  
311 through the Scenario S1, but also show some similarities (Fig. 9c and d). Most of the flow passes through  
312 the hydrograph profile O1 between  $t = t_0 + 40$  s and  $t_0 + 80$  s, and through O2 between  $t = t_0 + 100$  s and

313  $t_0 + 180$  s. The hydrograph OH2 is characterized by a short peak of 3,500 m<sup>3</sup>/s of solid and 4,500 m<sup>3</sup>/s of  
314 fluid, with a volumetric solid fraction of 0.44 and quickly decreasing discharge afterwards (Fig. 9c). In  
315 contrast to Scenario S1, flow heights drop steadily, with values below 2 m from  $t = t_0 + 620$  s onwards.  
316 The hydrograph OH3 is characterized by a surge starting around  $t = t_0 + 240$  s. Discharge at the hydro-  
317 graph OH4 (Fig. 9d) sets on around  $t = t_0 + 600$  s, and the solid peak of 240 m<sup>3</sup>/s is simulated at approx.  
318  $t = t_0 + 780$  s. The delay of the peak of fluid discharge is more pronounced when compared to Scenario S1  
319 (310 m<sup>3</sup>/s at  $t = t_0 + 960$  s). Profile O4 is passed by a total of 65,000 m<sup>3</sup> of solid and 204,000 m<sup>3</sup> of fluid  
320 material. The volumetric solid fraction drops from above 0.60 at the very onset of the hydrograph to  
321 around 0.10 (almost pure fluid) at the end. The maximum total flow height at O4 is 3.1 m.

322 Fig. 12 illustrates the travel times and the frontal velocities of the rock avalanche and the initial debris  
323 flow. Assuming that  $t_0$  is in the range of some tens of seconds, the time of arrival of the surge at O3 is in  
324 line with the documentation also for the Scenario S2 (Fig. 12a; Table 3). The frontal velocity patterns  
325 along Val Bondasca are roughly in line with those derived in the Scenario S1 (Fig. 12b). However, the  
326 scenarios differ among themselves in terms of the more pronounced, but shorter peaks of the hydro-  
327 graphs in Scenario S2 (Fig. 9). This pattern is a consequence of the more sharply defined debris flow  
328 surge. In Scenario S1, the front of the rock avalanche deposit constantly “leaks” into Val Bondasca,  
329 providing supply for the debris flow also at later stages. In Scenario S2, entrainment of the rock ava-  
330 lanche deposit occurs relatively quickly, without material supply afterwards. This type of behaviour is  
331 strongly coupled to the value of  $C_E$  and the allowed height of entrainment chosen for the rock avalanche  
332 deposit.

## 333 6 Discussion

334 Our simulation results reveal a reasonable degree of empirical adequacy and physical plausibility with  
335 regard to most of the reference observations. Having said that, we have also identified some important  
336 limitations which are now discussed in more detail. First of all, we are not able to decide on the more  
337 realistic of the two Scenarios S1 and S2. In general, the melting and mobilization of glacier ice upon rock  
338 slide-rock fall impact is hard to quantify from straightforward calculations of energy transformation, as  
339 Huggel et al. (2005) have demonstrated on the example of the 2002 Kolka-Karmadon event. In the pre-  
340 sent work, the assumed amount of melting (approx. half of the glacier ice) leading to the empirically  
341 most adequate results corresponds well to the findings of WSL (2017), indicating a reasonable degree of  
342 plausibility. It remains equally difficult to quantify the amount of water injected into the rock avalanche  
343 by overload of the sediments and the resulting pore pressure rise (Walter et al., 2019). Confirmation or

344 rejection of conceptual models with regard to the physical mechanisms involved in specific cases would  
345 have to be based on better constrained initial conditions, and the availability of robust parameter sets.

346 We note that with the approach chosen we are not able (i) to adequately simulate the transition from  
347 solid to fluid material; and (ii) to consider rock and ice separately with different material properties,  
348 which would require a three-phase model, not within the scope here. Therefore, entrained ice is consid-  
349 ered viscous fluid from the beginning. A physically better founded representation of the initial phase of  
350 the event would require an extension of the flow model employed. Such an extension could build on the  
351 rock-ice avalanche model introduced by Pudasaini and Krautblatter (2014). Also the vertical patterns of  
352 the situation illustrated in Fig. 5 cannot be modelled with the present approach, which (i) does not con-  
353 sider melting of ice; and (ii) only allows one entrainable layer at each pixel. The assumption of fluid be-  
354 haviour of glacier ice therefore represents a necessary simplification which is supported by observations  
355 (Fig. 3b), but neglects the likely presence of remaining ice in the basal part of the eroded glacier, which  
356 melted later and so contributed to the successive debris flow surges.

357 Still, we currently consider the Pudasaini (2012) model – and the extended multi-phase model (Puda-  
358 saini and Mergili, 2019) – best practice, even though other two-phase or bulk mixture models do exist.  
359 Most recently, Iverson and George (2014) presented an approach that has been solved with an open  
360 source software, called D-Claw (George and Iverson, 2014), and compared to large-scale experiments  
361 considering dense debris materials (Iverson et al., 2000; Iverson et al., 2010). The Iverson and George  
362 (2014) model can be useful for very dense debris flows where the solid particles and fluid molecules  
363 move together. However, its applicability to cascading mass flows is limited for the following reasons: (i)  
364 this model assumes that the solid and fluid velocities are the same, an assumption that does not hold for  
365 complex, cascading mass flows; (ii) the pore fluid pressure evolution equation includes pore pressure  
366 advection and source terms associated with dilation, but ignores the pore fluid diffusion; (iii) there are  
367 no real interfacial momentum transfers, such as the drag force, virtual mass force, and buoyancy be-  
368 tween the solid and fluid phases; and (iv) neither viscous shear stress, nor dynamical coupling between  
369 the pore fluid pressure evolution and the bulk momentum equations are considered. Furthermore, as the  
370 fluid pressure evolution is assumed to play a substantial role in the Iverson and George (2014) model, the  
371 solid and fluid dynamics cannot be similar, and thus the assumption of negligible relative velocity be-  
372 tween solid and fluid is questionable (Pitman and Le, 2005; Pudasaini, 2012).

373 The initial rock slide-rock fall and the rock avalanche are simulated in a plausible way, at least with re-  
374 gard to the deposition area. Whereas the simulated deposition area is clearly defined in Scenario S2, this  
375 is to a lesser extent the case in Scenario S1, where the front of the rock avalanche directly transforms  
376 into a debris flow. Both scenarios seem to overestimate the time between release and deposition, com-

377 pared to the seismic signals recorded – an issue also reported by WSL (2017) for their simulation. We  
378 observe a relatively gradual deceleration of the simulated avalanche, without clearly defined stopping  
379 and note that also in the **Scenario S2**, there is some diffusion after the considered time of 120 s, so that  
380 the definition of the simulated deposit is somehow arbitrary. The elaboration of well-suited stopping  
381 criteria, going beyond the very simple approach introduced by Mergili et al. (2017), remains a task for  
382 the future. However, as the rock avalanche has already been successfully back-calculated by WSL  
383 (2017), we focus on the first debris flow surge: the simulation input is optimized towards the back-  
384 calculation of the debris flow volumes entering the valley at the hydrograph profile O2 (Table 3). The  
385 travel times to the hydrograph profiles O3 and O4 are reproduced in a plausible way in both scenarios,  
386 and so are the impact areas (**Figs. 8 and 11**). Exceedance of the lateral limits in the lower zones is at-  
387 tributed to an overestimate of the debris flow volumes there, and to numerical issues related to the nar-  
388 row gorge. **The same is true for the fan of Bondo.** The solid ratio of the debris flow in the simulations  
389 appears realistic, ranging around **40–45%** in the early stage of the debris flow, and around **30–35% and**  
390 **lower (depending on the cut-off time of the hydrograph)** in the final stage. This means that solid materi-  
391 al tends to stop in the transit area rather than fluid material, as it can be expected. Nevertheless, the cor-  
392 rect simulation of the deposition of debris flow material along Val Bondasca remains a major challenge  
393 (Table 3). Even though a considerable amount of effort was put in reproducing the much lower volumes  
394 reported in the vicinity of O4, the simulations result in an overestimate of the volumes passing through  
395 this hydrograph profile. This is most likely a consequence of the failure of r.avaflow to adequately re-  
396 produce the deposition pattern in the zones D and E. Whereas some material remains there at the end of  
397 the **simulation, more** work is necessary to appropriately understand the mechanisms of deposition in  
398 viscous debris flows (Pudasaini and Fischer, 2016b). Part of the discrepancy, however, might be ex-  
399 plained by the fact that part of the fluid material – which does not only consist of pure water, but of a  
400 mixture of water and fine mud – left the area of interest in downstream direction and was therefore not  
401 included in the reference measurements.

402 The simulation results are strongly influenced by the initial conditions and the model parameters. Pa-  
403 rameterization of both scenarios is complex and highly uncertain, particularly in terms of optimizing the  
404 volumes of entrained till and glacial meltwater, and injected pore water. In general, the parameter sets  
405 optimized to yield empirically adequate results are physically plausible, in contrast to Mergili et al.  
406 (2018b) who had to set the basal friction angle in a certain zone to a negligible value in order to repro-  
407 duce the observed overtopping of a more than 100 m high ridge (1970 Huascarán landslide). In contrast,  
408 reproducing the travel times to O4 in the present study requires the assumption of a low mobility of the  
409 flow in Zone E. This is achieved by increasing the friction (Table 1), accounting for the narrow flow



410 channel, i.e. the interaction of the flow with the channel walls, which is not directly accounted for in  
411 r.avaflow. Still, the high values of  $\delta$  given in Table 1 are not directly applied, as they scale with the **solid**  
412 **fraction**. This type of weighting has to be further scrutinized. We emphasize that also reasonable param-  
413 eter sets are not necessarily **physically** true, as the large number of parameters involved (Tables 1 and 2)  
414 creates a lot of space for equifinality issues (Beven et al., 1996).

415 We have further shown that the classical evaluation of empirical adequacy, by comparing observed and  
416 simulated impact areas, is not enough in the case of complex mass flows: travel times, hydrographs, and  
417 volumes involved can provide important insight in addition to the classical quantitative performance  
418 indicators used, for example, in landslide susceptibility modelling (Formetta et al., 2015). Further, the  
419 delineation of the observed impact area is uncertain as the boundary of the event is not clearly defined  
420 particularly in Zone C.

421 The present work is seen as a further step towards a better understanding of the challenges and the pa-  
422 rameterization concerning the integrated simulation of complex mass flows. More case studies are neces-  
423 sary to derive guiding parameter sets facilitating predictive simulations of such events (Mergili et al.,  
424 2018a, b). A particular challenge of such case studies consists in the parameter optimization procedure:  
425 in principle, automated methods do exist (e.g. Fischer, 2013). However, they have been developed for  
426 optimizing globally defined parameters (which are constant over the entire study area) against runoff  
427 length and impact area, and such tools do a very good job for exactly this purpose. However, they cannot  
428 directly deal with spatially variable parameters, as they are defined in the present work. With some  
429 modifications they might even serve for that – but the main issue is that optimization also considers  
430 shapes and maximum values of hydrograph discharges, or travel times at different places of the path. It  
431 would be a huge effort to trim optimization algorithms to this purpose, and to make them efficient  
432 enough to prevent excessive computational times – we consider this as an important task for the future  
433 which is out of scope of the present work. Therefore, we have used a step-wise expert-based optimiza-  
434 tion strategy.

## 435 7 Conclusions

436 Both of the investigated Scenarios S1 (debris flow developing at the front of the rock avalanche) and S2  
437 (debris flow developing at the back of the rock avalanche, overtopping the deposit) lead to empirically  
438 reasonably adequate results, when back calculated with r.avaflow using physically plausible model pa-  
439 rameters. Based on the simulations performed in the present study, final conclusions on the more likely  
440 of the mechanisms sketched in Fig. 6 can therefore not be drawn purely based on the simulations. The

441 observed jet of glacial meltwater (Fig. 3b) points towards **Scenario S1**. The observed scouring of the rock  
442 avalanche deposit, in contrast, rather points towards **Scenario S2**, but could also be associated to subse-  
443 quent debris flow surges. Open questions include at least (i) the interaction between the initial rock  
444 slide-rock fall and the glacier; (ii) flow transformations in the lower portion of Zone C (**Fig. 7**), leading to  
445 the first debris flow surge; and (iii) the mechanisms of deposition of 90% of the debris flow material  
446 along the flow channel in the Val Bondasca. Further research is therefore urgently needed to shed more  
447 light on this extraordinary landslide cascade in the Swiss Alps. In addition, improved simulation con-  
448 cepts are needed to better capture the dynamics of complex landslides in glacierized environments: such  
449 would particularly have to include three-phase models, where ice – and melting of ice – are considered  
450 in a more explicit way. **Finally, more case studies of complex mass flows have to be performed in order**  
451 **to derive guiding parameter sets serving for predictive simulations.**

## 452 **Code availability**

453 The `r.avaflow` code, including a detailed manual, is available for download at the `r.avaflow` website  
454 (Mergili and Pudasaini, 2019).

## 455 **Data availability**

456 The study is largely based on the 2011 swisstopo MNS-Digital Elevation Model (DEM) (contract: swis-  
457 stopo–DV084371), and derivatives thereof. Unfortunately, the authors are not entitled to make these  
458 data publicly available.

459

## 460 **Author contributions**

461 Martin Mergili (MM), Michel Jaboyedoff (MJ), José Pullarello (JP), Shiva P. Pudasaini (SP)

462 MM has contributed to the conceptualization and methodology of the research, designed the software,  
463 and performed the formal analysis, visualization, validation, and most of the writing of the original draft.

464 MJ was involved in the conceptualization, investigation, and supervision as well as in the review and  
465 editing of the manuscript. JP has contributed to the investigation, visualization, and review & editing. SP  
466 has provided input in terms of methodology and review & editing of the manuscript.

## 467 **Competing interests**

468 The authors declare that they have no conflict of interest.

## 469 **Acknowledgements**

470 Shiva P. Pudasaini gratefully thanks the Herbette Foundation for providing financial support for his sab-  
471 batical visit to the University of Lausanne, Switzerland in the period April–June 2018, where this con-  
472 tribution was triggered. Similarly, this work has been financially supported by the German Research  
473 Foundation (DFG) through the research project PU 386/5-1: “A novel and unified solution to multi-  
474 phase mass flows”. It strongly builds on the outcomes of the international cooperation project “A GIS  
475 simulation model for avalanche and debris flows (avaflow)” supported by the German Research Founda-  
476 tion (DFG, project number PU 386/3-1) and the Austrian Science Fund (FWF, project number I 1600-  
477 N30).

478 We would like to thank Brian McArdell and another anonymous reviewer for providing constructive  
479 comments and suggestions that helped to enhance the paper substantially, and are grateful to Sophia  
480 Demmel and Florian Amann for valuable discussions and to Matthias Benedikt for comprehensive tech-  
481 nical assistance.

## 482 **References**

- 483 Amann, F., Kos, A., Phillips, M., and Kenner, R.: The Piz Cengalo Bergsturz and subsequent debris flows,  
484 *Geophys. Res. Abstr.*, 20, 14700, 2018.
- 485 Amt für Wald und Naturgefahren: Bondo: Chronologie der Ereignisse, 2 pp.,  
486 [https://www.gr.ch/DE/institutionen/verwaltung/bvfd/awn/dokumentenliste\\_afw/20170828\\_Chronologie](https://www.gr.ch/DE/institutionen/verwaltung/bvfd/awn/dokumentenliste_afw/20170828_Chronologie_Bondo_2017_12_13_dt.pdf)  
487 [\\_Bondo\\_2017\\_12\\_13\\_dt.pdf](https://www.gr.ch/DE/institutionen/verwaltung/bvfd/awn/dokumentenliste_afw/20170828_Chronologie_Bondo_2017_12_13_dt.pdf), accessed on 31 May 2019.
- 488 Beven, K.: Equifinality and Uncertainty in Geomorphological Modelling, in: *The Scientific Nature of*  
489 *Geomorphology: Proceedings of the 27th Binghamton Symposium in Geomorphology, 27-29 September*  
490 *1996*, John Wiley & Sons, 289–313, 1996.
- 491 Bonanomi, Y., and Keiser, M.: Bericht zum aktuellen Bergsturz am Piz Cengalo 2017, Bergeller Alpen im  
492 Engadin, 19. Geoforum Umhausen, 19.–20. Oktober 2017, 55–60, 2017.
- 493 Christen, M., Kowalski, J., and Bartelt, P.: RAMMS: Numerical simulation of dense snow avalanches in  
494 three-dimensional terrain, *Cold Reg. Sci. Technol.*, 63, 1–14,  
495 <https://doi.org/10.1016/j.coldregions.2010.04.005>, 2010.

496 De Blasio, F. V., and Crosta, G. B.: Extremely Energetic Rockfalls: Some preliminary estimates, in: Land-  
497 slides and Engineered Slopes. Experience, Theory and Practice, 759–764, CRC Press, 2016.

498 Demmel, S.: Water Balance in Val Bondasca. Initial hydrological conditions for debris flows triggered by  
499 the 2017 rock avalanche at Pizzo Cengalo. Master Thesis, ETH Zurich, 50 pp., 2019.

500 Domnik, B., Pudasaini, S. P., Katzenbach, R., and Miller, S. A.: Coupling of full two-dimensional and  
501 depth-averaged models for granular flows, *J. Non-Newtonian Fluid Mech.*, 201, 56–68,  
502 <https://doi.org/10.1016/j.jnnfm.2013.07.005>, 2013.

503 Evans, S. G., Bishop, N.F., Fidel Smoll, L., Valderrama Murillo, P., Delaney, K.B., and Oliver-Smith, A.:  
504 A re-examination of the mechanism and human impact of catastrophic mass flows originating on Neva-  
505 do Huascarán, Cordillera Blanca, Peru in 1962 and 1970, *Eng. Geol.*, 108, 96–118,  
506 <https://doi.org/10.1016/j.enggeo.2009.06.020>, 2009.

507 Fischer, J.-T., Kowalski, J., and Pudasaini, S. P.: Topographic curvature effects in applied avalanche mod-  
508 eling, *Cold Reg. Sci. Technol.*, 74, 21–30, <https://doi.org/10.1016/j.coldregions.2012.01.005>, 2012.

509 Fischer, J.-T., Kofler, A., Fellin, W., Granig, M., and Kleemayr, K.: Multivariate parameter optimization  
510 for computational snow avalanche simulation in 3d terrain, *J. Glaciol.*, 61(229), 875–888,  
511 <https://doi.org/10.3189/2015JoG14J168>, 2015.

512 Formetta, G., Capparelli, G., and Versace, P.: Evaluating performances of simplified physically based  
513 models for landslide susceptibility, *Hydrol. Earth Syst. Sci. Discuss.*, 12, 13217–13256,  
514 <https://doi.org/10.5194/hessd-19-1-2015>, 2015.

515 Frank, F., Huggel, C., McArdeall, B. W., and Vieli, A.: Landslides and increased debris-flow activity: a  
516 systematic comparison of six catchments in Switzerland. *Earth Surf. Proc. Landforms*, 44(3), 699–712,  
517 <https://doi.org/10.1002/esp.4524>, 2019.

518 George, D. L., and Iverson, R. M.: A depth-averaged debris-flow model that includes the effects of evolu-  
519 ting dilatancy. II. Numerical predictions and experimental tests. *Proc. Royal Soc. A*, 470(2170), 20130820,  
520 <https://doi.org/10.1098/rspa.2013.0820>, 2014.

521 Haeberli, W.: Mountain permafrost—research frontiers and a special long-term challenge, *Cold Reg. Sci.*  
522 *Technol.*, 96, 71–76, <https://doi.org/10.1016/j.coldregions.2013.02.004>, 2013.

523 Haeberli, W., and Whiteman, C. (Eds.): *Snow and Ice-related Hazards, Risks and Disasters*, Elsevier,  
524 <https://doi.org/10.1016/B978-0-12-394849-6.00001-9>, 2014.

525 Haeberli, W., Schaub, Y., and Huggel, C.: Increasing risks related to landslides from degrading perma-  
526 frost into new lakes in de-glaciating mountain ranges, *Geomorphology*, 293(B), 405–417,  
527 <https://doi.org/10.1016/j.geomorph.2016.02.009>, 2017.

528 Harris, C., Arenson, L. U., Christiansen, H. H., Etzelmüller, B., Frauenfelder, R., Gruber, S., Haeberli,  
529 W., Hauck, C., Hölzle, M., Humlum, O., Isaksen, K., Kääb, A., Kern-Lütschg, M. A., Lehning, M., Mat-  
530 suoka, N., Murton, J. B., Nötzli, J., Phillips, M., Ross, N., Seppälä, M., Springman, S. M., and Vonder  
531 Mühl, D.: Permafrost and climate in Europe: Monitoring and modelling thermal, geomorphological and  
532 geotechnical responses, *Earth-Sci. Rev.*, 92, 117–171, <https://doi.org/10.1016/j.earscirev.2008.12.002>,  
533 2009.

534 Hewitt, K.: Styles of rock-avalanche depositional complexes conditioned by very rugged terrain, Karako-  
535 ram Himalaya, Pakistan, *Rev. Eng. Geol.*, 15, 345–377, 2002.

536 Huggel, C., Zraggen-Oswald, S., Haeberli, W., Kääb, A., Polkvoj, A., Galushkin, I., and Evans, S.G.: The  
537 2002 rock/ice avalanche at Kolka/Karmadon, Russian Caucasus: assessment of extraordinary avalanche  
538 formation and mobility, and application of QuickBird satellite imagery, *Nat. Hazards Earth Syst. Sci.*, 5,  
539 173–187, <https://doi.org/10.5194/nhess-5-173-2005>, 2005.

540 Iverson, R. M.: The physics of debris flows, *Rev. Geophys.*, 35, 245–296,  
541 <https://doi.org/10.1029/97RG00426>, 1997.

542 Iverson, R. M., Reid, M. E., Iverson, N. R., LaHusen, R. G., Logan, M., Mann, J. E., and Brien, D. L.:  
543 Acute sensitivity of landslide rates to initial soil porosity, *Science*, 290, 513–516,  
544 <https://doi.org/10.1126/science.290.5491.513>, 2000.

545 Iverson, R. M., Logan, M., LaHusen, R. G., and Berti, M.: The perfect debris flow? aggregated results  
546 from 28 large-scale experiments, *J. Geophys. Res.*, 115, 1–29, <https://doi.org/10.1029/2009JF001514>, 2010.

547 Iverson, R. M., and George, D. L.: A depth-averaged debris-flow model that includes the effects of evol-  
548 ving dilatancy. I. Physical basis, *Proc. Royal Soc. A*, 470(2170), 20130819,  
549 <https://doi.org/10.1098/rspa.2013.0819>, 2014.

550 Kattel, P., Khattri, K. B., Pokhrel, P. R., Kafle, J., Tuladhar, B. M., and Pudasaini, S. P.: Simulating glacial  
551 lake outburst floods with a two-phase mass flow model, *Ann. Glaciol.*, 57(71), 349–358,  
552 <https://doi.org/10.3189/2016AoG71A039>, 2016.

553 Krautblatter, M., Funk, D., and Günzel, F. K.: Why permafrost rocks become unstable: a rock-ice-  
554 mechanical model in time and space, *Earth Surf. Process. Landf.*, 38, 876–887,  
555 <https://doi.org/10.1002/esp.3374>, 2013.

556 McDougall, S., and Hungr, O.: A Model for the Analysis of Rapid Landslide Motion across Three-  
557 Dimensional Terrain, *Can. Geotech. J.*, 41, 1084–1097, <https://doi.org/10.1139/t04-052>, 2004.

558 Mergili, M., Pudasaini, S. P.: r.avaflow – The open source mass flow simulation model,  
559 <https://www.avaflow.org/>, last access: 7 July 2019.

560 Mergili, M., Fischer, J.-T., Krenn, J., and Pudasaini, S. P.: r.avaflow v1, an advanced open source compu-  
561 tational framework for the propagation and interaction of two-phase mass flows, *Geosci. Model Dev.*, 10,  
562 553–569, <https://doi.org/10.5194/gmd-10-553-2017>, 2017.

563 Mergili, M., Emmer, A., Juřicová, A., Cochachin, A., Fischer, J.-T., Huggel, C., and Pudasaini, S.P.: How  
564 well can we simulate complex hydro-geomorphic process chains? The 2012 multi-lake outburst flood in  
565 the Santa Cruz Valley (Cordillera Blanca, Perú), *Earth Surf. Process. Landf.*, 43(7), 1373–1389,  
566 <https://doi.org/10.1002/esp.4318>, 2018a.

567 Mergili, M., Frank, B., Fischer, J.-T., Huggel, C., and Pudasaini, S. P.: Computational experiments on the  
568 1962 and 1970 landslide events at Huascarán (Peru) with r.avaflow: Lessons learned for predictive mass  
569 flow simulations, *Geomorphology*, 322, 15–28, <https://doi.org/10.1016/j.geomorph.2018.08.032>, 2018b.

570 Nesyahu, H., and Tadmor, E.: Non-oscillatory central differencing for hyperbolic conservation laws, *J.*  
571 *Comput. Phys.*, 87, 408–463, [https://doi.org/10.1016/0021-9991\(90\)90260-8](https://doi.org/10.1016/0021-9991(90)90260-8), 1990.

572 Nicoletti, G. P., and Sorriso-Valvo, M.: Geomorphic controls of the shape and mobility of rock ava-  
573 lanches, *GSA Bull.*, 103(10), 1365–1373, [https://doi.org/10.1130/0016-7606\(1991\)103<1365:GCOTSA>2.3.CO;2](https://doi.org/10.1130/0016-7606(1991)103<1365:GCOTSA>2.3.CO;2), 1991.

575 Pitman, E.B., and Le, L.: A two-fluid model for avalanche and debris flows. *Philos. Trans. R. Soc. A*, 363,  
576 1573–1601, <https://doi.org/10.1098/rsta.2005.1596>, 2005.

577 Pudasaini, S. P.: A general two-phase debris flow model, *J. Geophys. Res. Earth Surf.*, 117, F03010,  
578 <https://doi.org/10.1029/2011JF002186>, 2012.

579 Pudasaini, S. P.: A full description of generalized drag in mixture mass flows, *Phys. Fluids*, submitted  
580 manuscript, 2019.

581 Pudasaini, S. P., and Krautblatter, M.: A two-phase mechanical model for rock-ice avalanches, *J. Ge-*  
582 *ophys. Res. Earth Surf.*, 119, doi:10.1002/2014JF003183, 2014.

583 Pudasaini, S. P., and Fischer, J.-T.: A mechanical model for phase-separation in debris flow,  
584 arXiv:1610.03649, 2016a.

585 Pudasaini, S.P., and Fischer, J.-T.: A mechanical erosion model for two-phase mass flows,  
586 arXiv:1610.01806, 2016b.

587 Pudasaini, S.P., and Mergili, M.: A Multi-Phase Mass Flow Model, *J. Geophys. Res. Earth Surf.*,  
588 JGRF21102, <https://doi.org/10.1029/2019JF005204>, 2019.

589 Preh, A., and Sausgruber, J. T.: The Extraordinary Rock-Snow Avalanche of Alpl, Tyrol, Austria. Is it  
590 Possible to Predict the Runout by Means of Single-phase Voellmy- or Coulomb-Type Models?, in: *Engi-  
591 neering Geology for Society and Territory–Volume 2*, edited by: Lollino, G. et al., Springer, Cham,  
592 [https://doi.org/10.1007/978-3-319-09057-3\\_338](https://doi.org/10.1007/978-3-319-09057-3_338), 2015.

593 Saltelli, A., and Annoni, P.: How to avoid a perfunctory sensitivity analysis, *Environ. Model. Softw.*, 25,  
594 1508–1517, <https://doi.org/10.1016/j.envsoft.2010.04.012>, 2010.

595 Savage, S. B., and Hutter, K.: The motion of a finite mass of granular material down a rough incline, *J.*  
596 *Fluid Mech.*, 199, 177–215, <https://doi.org/10.1017/S0022112089000340>, 1989.

597 Scheidegger, A. E.: On the Prediction of the Reach and Velocity of Catastrophic Landslides, *Rock Mech.*,  
598 5, 231–236, <https://doi.org/10.1007/BF01301796>, 1973.

599 Schneider, D., Huggel, C., Cochachin, A., Guillén, S., and García, J.: Mapping hazards from glacier lake  
600 outburst floods based on modelling of process cascades at Lake 513, Carhuaz, Peru, *Adv. Geosci.*, 35,  
601 145–155, <https://doi.org/10.5194/adgeo-35-145-2014>, 2014.

602 Somos-Valenzuela, M. A., Chisolm, R. E., Rivas, D. S., Portocarrero, C., and McKinney, D. C.: Modeling  
603 a glacial lake outburst flood process chain: the case of Lake Palcacocha and Huaraz, Peru, *Hydrol. Earth  
604 Syst. Sci.*, 20, 2519–2543, <https://doi.org/10.5194/hess-20-2519-2016>, 2016.

605 Steinacher, R., Kuster, C., Buchli, C., and Meier, L.: The Pizzo Cengalo and Val Bondasca events: From  
606 early warnings to immediate alarms, *Geophys. Res. Abstr.* 20, 17536, 2018.

607 Tai, Y. C., Noelle, S., Gray, J. M. N. T., and Hutter, K.: Shock-capturing and front-tracking methods for  
608 granular avalanches, *J. Comput. Phys.*, 175(1), 269–301, <https://doi.org/10.1006/jcph.2001.6946>, 2002.

609 VAW: Vadrec dal Cengal Ost: Veränderungen in Vergangenheit und Zukunft. Laboratory of Hydraulics,  
610 Hydrology and Glaciology of the Swiss Federal Institute of Technology Zurich, 17 pp.,  
611 [https://www.gr.ch/DE/institutionen/verwaltung/bvfd/awn/dokumentenliste\\_afw/Cengalo%20Gletschere  
612 ntwicklung%20ETH\\_2nov\\_final.pdf](https://www.gr.ch/DE/institutionen/verwaltung/bvfd/awn/dokumentenliste_afw/Cengalo%20Gletschere), accessed on 31 May 2019, 2017.

613 Voellmy, A.: Über die Zerstörungskraft von Lawinen, *Schweizerische Bauzeitung*, 73, 159–162, 212–217,  
614 246–249, 280–285, 1955.

615 Walter, F., Wenner, M., and Amann, F.: Seismic Analysis of the August 2017 Landslide on Piz Cengalo  
616 (Switzerland), *Geophys. Res. Abstr.*, 20, 3163-1, 2018.

617 Walter, F., Amann, F., Kos, A., Kenner, R., Phillips, M., de Preux, A., Huss, M., Tognacca, C., Clinton, J.,  
618 Diehl, T., and Bonanomi, Y.: Direct observations of a three million cubic meter rock-slope collapse with  
619 almost immediate initiation of ensuing debris flows, *Earth Planet. Sci. Lett.*, submitted manuscript, 2019.

620 Wang, Y., Hutter, K., and Pudasaini, S. P.: The Savage-Hutter theory: A system of partial differential  
621 equations for avalanche flows of snow, debris, and mud, *ZAMM – J. Appl. Math. Mech.*, 84(8), 507–527,  
622 <https://doi.org/10.1002/zamm.200310123>, 2004.

623 Worni, R., Huggel, C., Clague, J. J., Schaub, Y., and Stoffel, M.: Coupling glacial lake impact, dam  
624 breach, and flood processes: A modeling perspective, *Geomorphology*, 224, 161–176,  
625 <https://doi.org/10.1016/j.geomorph.2014.06.031>, 2014.

626 WSL.: SLF Gutachten G2017.20: Modellierung des Cengalo Bergsturzes mit verschiedenen Rahmenbe-  
627 dingungen, Bondo, GR. WSL-Institut für Schnee- und Lawinenforschung SLF, 69 pp.,  
628 [https://www.gr.ch/DE/institutionen/verwaltung/bvfd/awn/dokumentenliste\\_afw/SLF\\_G2017\\_20\\_Modell](https://www.gr.ch/DE/institutionen/verwaltung/bvfd/awn/dokumentenliste_afw/SLF_G2017_20_Modellierung_Cengalo_Bergsturz_030418_A.pdf)  
629 [ierung\\_Cengalo\\_Bergsturz\\_030418\\_A.pdf](https://www.gr.ch/DE/institutionen/verwaltung/bvfd/awn/dokumentenliste_afw/SLF_G2017_20_Modellierung_Cengalo_Bergsturz_030418_A.pdf), accessed on 31 May 2019, 2017.

630



631 **Tables**

632 Table 1. Descriptions and optimized parameter values for each of the zones A–F (Fig. 4 and Fig. 7). The  
 633 names of the model parameters are given in the text and in Table 2. The values provided in Table 2 are  
 634 assigned to those parameters not shown. (S1) and (S2) refer to the corresponding scenarios. Explanations  
 635 of the superscripts: <sup>1)</sup> Note that in all zones and in both of the scenarios S1 and S2,  $\delta$  is assumed to scale  
 636 linearly with the solid fraction. This means that the values given only apply in case of 100% solid. <sup>2)</sup> This  
 637 only applies to the initial landslide, which is assumed completely dry in Scenario S2. Due to the scaling  
 638 of  $\delta$  with the solid fraction, a lower basal friction is required to obtain results similar to Scenario S1,  
 639 where the rock avalanche contains some fluid. The same values of  $\delta$  as for Scenario S1 are applied for the  
 640 debris flow in Scenario S2 throughout all zones. <sup>3)</sup> This volume is derived from our own reconstruction  
 641 (Fig. 5). In contrast, WSL (2017) gives 3.1 million m<sup>3</sup>, and Amann et al. (2018) 3.15 million m<sup>3</sup>. <sup>4)</sup> In Sce-  
 642 nario S2, the glacier is not directly entrained, but instead released behind the rock avalanche. In both  
 643 scenarios, ice is considered to melt immediately on impact and included in the viscous fluid fraction. See  
 644 text for more detailed explanations.

Zone	Description	Model parameters	Initial conditions
A	Rock zone – NE face of Piz Cengalo with rock slide-rock fall release area	$\delta = 20^\circ$ (S1) <sup>1)</sup> $\delta = 13^\circ$ (S2) <sup>2)</sup> $C_{AD} = 0.2$	Release volume: 3.2 million m <sup>3</sup> , 100 % solid <sup>3)</sup>
B	Glacier zone – Cirque glacier beneath zone A, entrainment of glacier ice <sup>1)</sup>	$\delta = 20^\circ$ (S1) $\delta = 13^\circ$ (S2) $C_E = 10^{-6.5}$	Entrainment of glacier ice and till (Table 3) <sup>4)</sup>
C	Slope zone – steep, partly debris-covered glacier forefield leading down to the Val Bondasca	$\delta = 20^\circ$ (S1) $\delta = 13^\circ$ (S2) $C_E = 10^{-6.5}$ (S1) $C_E = 10^{-8.0}$ (S2)	Entrainment of injected water in Scenario S1 Entrainment of rock avalanche deposit in Scenario S2
D	Upper Val Bondasca zone – clearly defined flow channel becoming narrower in downstream direction	$\delta = 20-45^\circ$	No entrainment allowed, increasing friction
E	Lower Val Bondasca zone – narrow gorge	$\delta = 45^\circ$ $C_{FF} = 0.5$	No entrainment allowed, high friction due to lateral confinement
F	Bondo zone – deposition of the debris flow on the cone of Bondo	$\delta = 20^\circ$	No entrainment allowed

645

646 Table 2. Model parameters used for the simulations. Explanations of the superscripts: <sup>1)</sup> Fluid is here con-  
 647 sidered as a mixture of water and fine particles. This explains the higher density, compared to pure wa-  
 648 ter. <sup>2)</sup> The internal friction angle  $\varphi$  always has to be larger than or equal to the basal friction angle  $\delta$ .  
 649 Therefore, in case of  $\delta > \varphi$ ,  $\varphi$  is increased accordingly.

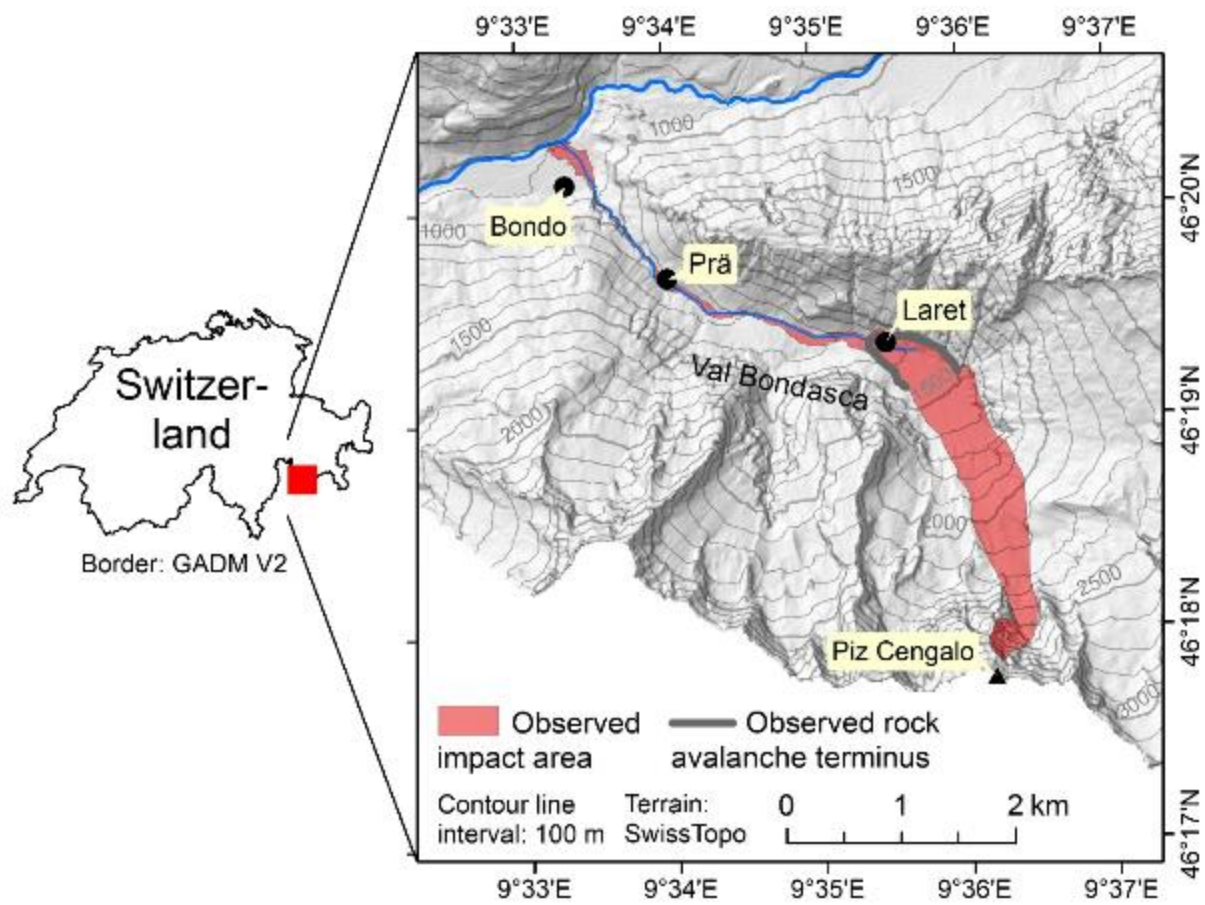
Symbol	Parameter	Unit	Value
$\rho_S$	Solid material density (grain density)	kg m <sup>-3</sup>	2,700
$\rho_F$	Fluid material density	kg m <sup>-3</sup>	1,400 <sup>1)</sup>
$\varphi$	Internal friction angle	Degree	27 <sup>2)</sup>
$\delta$	Basal friction angle	Degree	Table 1
$\nu$	Kinematic viscosity of the fluid	m <sup>2</sup> s <sup>-1</sup>	10
$\tau_Y$	Yield strength of the fluid	Pa	10
$C_{AD}$	Ambient drag coefficient	–	0.04 (exceptions in Table 1)
$C_{FF}$	Fluid friction coefficient	–	0.0 (exceptions in Table 1)
$C_E$	Entrainment coefficient	–	Table 1

650

651 Table 3. Selected output parameters of the simulations for the Scenarios S1 and S2 compared to the ob-  
652 served or documented parameter values. S = solid; F = fluid; fractions are expressed in terms of volume;  
653  $t_0$  = time from the initial release to the release of the first debris flow surge. Reference values are extract-  
654 ed from Amt für Wald und Naturgefahren (2017a), Bonanomi and Keiser (2017), and WSL (2017). \*\*\* =  
655 empirically adequate (within the documented range of values); \*\* = empirically partly adequate (less than  
656 50% away from the documented range of values); \* = empirically inadequate (at least 50% away from the  
657 documented range of values). The arithmetic means of minimum and maximum of each range are used  
658 for the calculations. Explanations of the superscripts: <sup>1)</sup> Not all the material entrained from the glacier  
659 was relevant for the first debris flow surge (Fig. 6), therefore lower volumes of entrained S (coarse till, in  
660 Scenario S2 also rock avalanche deposit) and F (molten ice and fine till, in Scenario S1 also pore water)  
661 yield the empirically most adequate results. The F volumes originating from the glacier in the simula-  
662 tions represent approx. half of the water equivalent of the entrained ice, corresponding well to the find-  
663 ings of WSL (2017). <sup>2)</sup> This value does not include the 145,000 m<sup>3</sup> of solid material remobilized through  
664 entrainment from the rock avalanche deposit in Scenario S2. <sup>3)</sup> WSL (2017) states that the rock ava-  
665 lanche came to rest approx. 60 s after release, whereas the seismic signals ceased 90 s after release. <sup>4)</sup> A  
666 certain time (here, we assume a maximum of 30 s) has to be allowed for the initial debris flow surge to  
667 reach O2, located slightly downstream of the front of the rock avalanche deposit. <sup>5)</sup> WSL (2017) gives a  
668 travel time of 3.5 minutes to Prä, roughly corresponding to the location of O3. It remains unclear  
669 whether this number refers to the release of the initial rock slide-rock fall or (more likely) to the start of  
670 the first debris flow surge. Bonanomi and Keiser (2017) give a travel time of roughly four minutes be-  
671 tween the initial release and the arrival of the first surge at the sensor of Prä. <sup>6)</sup> Amt für Wald und  
672 Naturgefahren (2017) gives a time span of 17 minutes between the release of the initial rock slide-rock  
673 fall and the arrival of the first debris flow surge at the “bridge” in Bondo. However, it is not indicated to  
674 which bridge this number refers. WSL (2017), in contrast, give a travel time of 7–8 minutes from Prä to  
675 the “old bridge” in Bondo, which, in sum, results in a shorter total travel time as indicated in Amt für  
676 Wald und Naturgefahren (2017). Depending on the bridge, the reference location for these numbers  
677 might be downstream from O4. In the simulation, this hydrograph shows a slow onset – travel times  
678 refer to the point when 5% of the total peak discharge are reached.

Parameter	Documenta- tion/Observation	Scenario S1	Scenario S2
Entrained ice (m <sup>3</sup> )	600,000 <sup>1)</sup>	–	–
Entrained S (m <sup>3</sup> )	–	60,000	60,000 <sup>2)</sup>
Entrained F (m <sup>3</sup> )	–	305,000	240,000
Duration of initial landslide (s)	60–90 <sup>3)</sup>	100–120**	100–120**
Travel time to O2 (s)	90–120 <sup>4)</sup>	140**	$t_0+120$ ***
Travel time to O3 (s)	210–300 <sup>5)</sup>	280***	$t_0+240$ ***
Travel time to O4 (s)	630–1020 <sup>6)</sup>	700***	$t_0+640$ ***
Debris flow volume at O2 (m <sup>3</sup> )	540,000	530,000** (43% S)	430,000** (45% S)
Debris flow volume at O4 (m <sup>3</sup> )	50,000	265,000* (34% S)	270,000* (24% S)

679



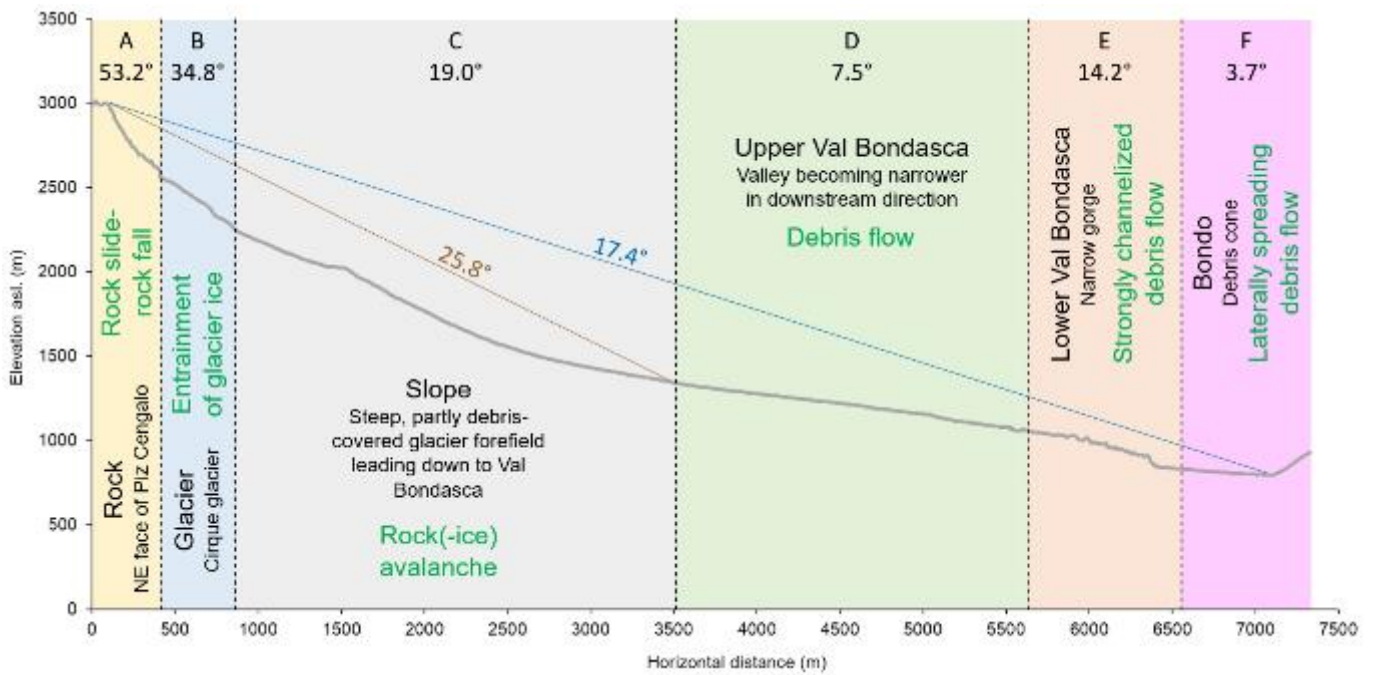
681 **Figure 1.** Study area with the impact area of the 2017 Piz Cengalo-Bondo landslide cascade. The ob-  
682 served rock avalanche terminus was derived from WSL (2017).  
683  
684



685  
686 Figure 2. Oblique view of the impact area of the event, orthophoto draped over the 2011 DTM. Data  
687 sources: swisstopo.  
688

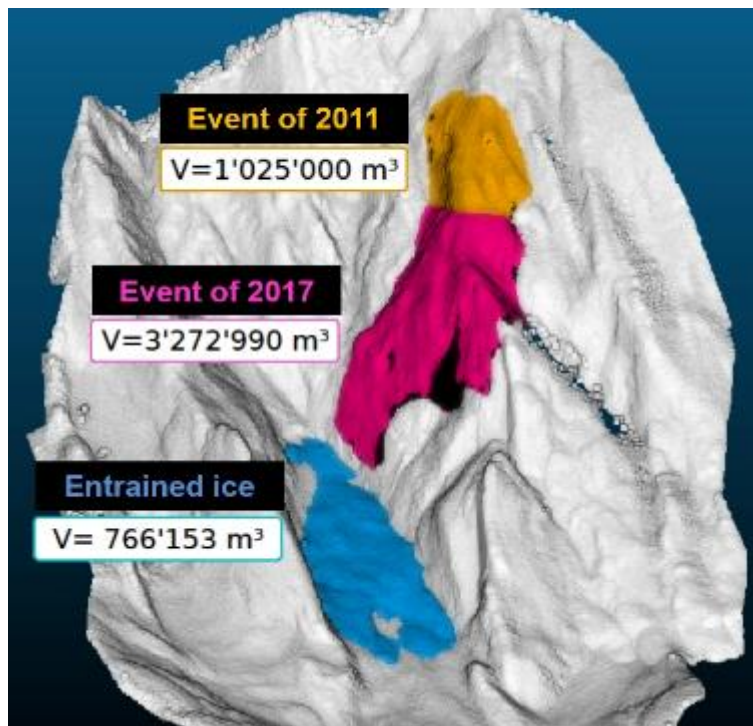


689  
 690 Figure 3. The 2017 Piz Cengalo-Bondo landslide cascade. (a) Scarp area on 20 September 2014. (b) Scarp  
 691 area on 23 September 2017 at 9:30, 20 s after release, frame of a video taken from the Capanna di Sciora.  
 692 Note the fountain of water and/or crushed ice at the front of the avalanche, most likely representing  
 693 meltwater from the impacted glacier. (c) Upper part of the Val Bondasca, where the channelized debris  
 694 flow developed. Note the zone of dust and pressure-induced damages to trees on the right side of the  
 695 valley. (d) Traces of the debris flows in the Val Bondasca. (e) The debris cone of Bondo after the event.  
 696 Image sources: Daniele Porro (a), Diego Salasc (b), VBS swisstopo Flugdienst (c)–(e).



697  
698  
699  
700  
701  
702  
703  
704

Figure 4. Profile along the main flow path of the Piz Cengalo-Bondo landslide cascade. The letters A–F indicate the individual zones (Table 1 and Fig. 7), whereas the associated numbers indicate the average angles of reach along the profile for each zone. The brown number and line show the angle of reach of the initial landslide (rock slide-rock fall and rock(-ice) avalanche), whereas the blue number and line show the angle of reach of the entire landslide cascade. The geomorphic characteristics of the zone (in black) are indicated along with the dominant process type (in green).

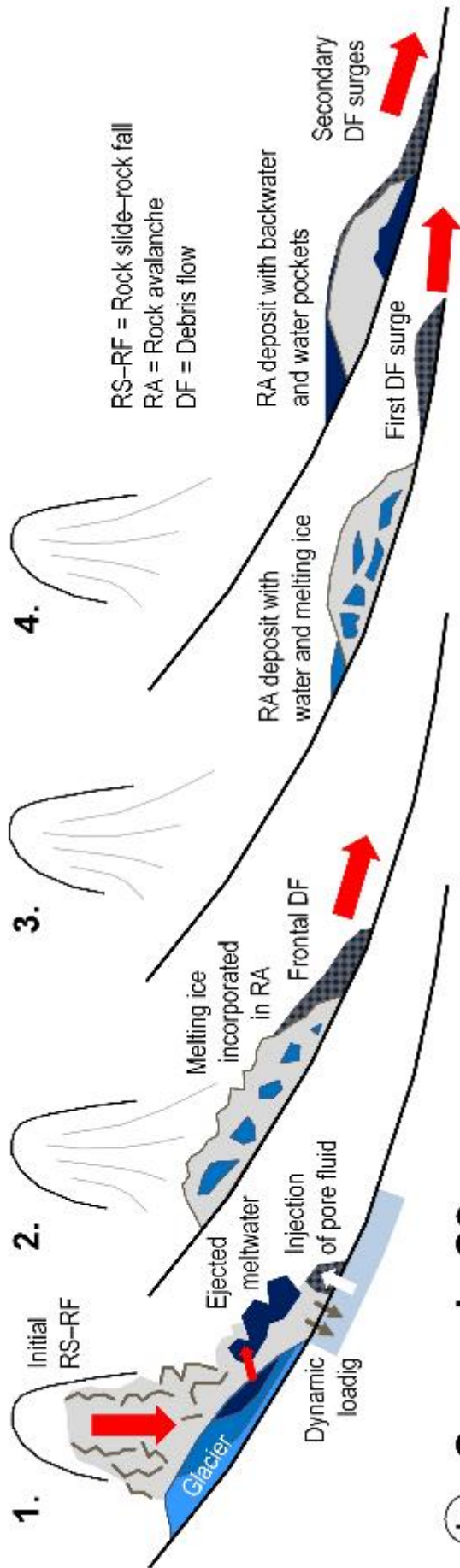


705  
 706  
 707  
 708  
 709  
 710  
 711

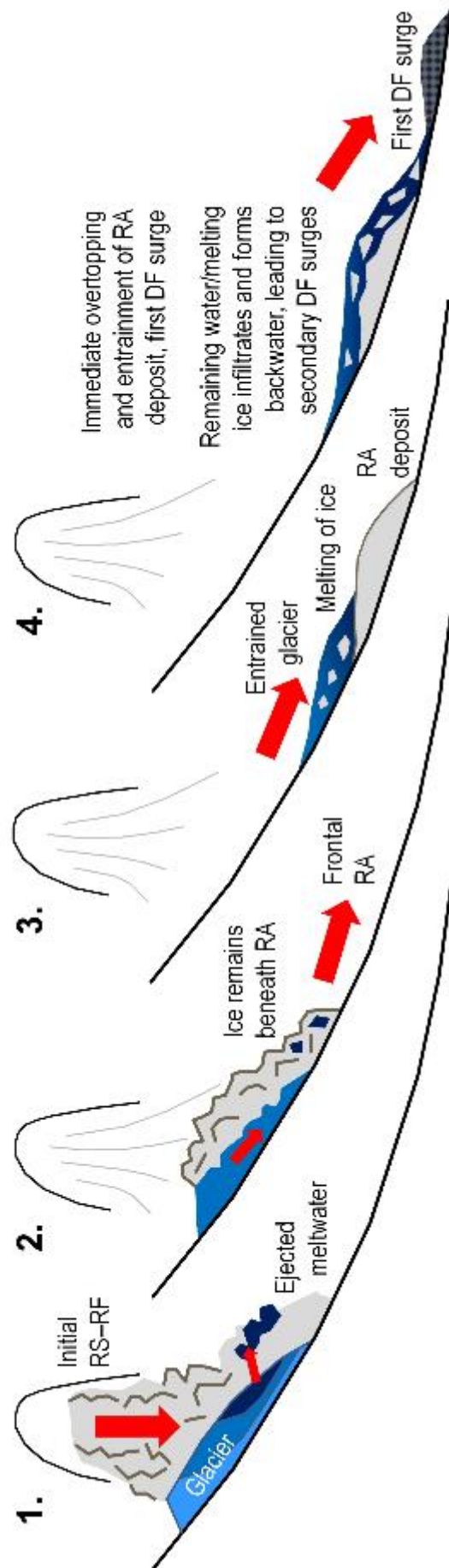
**Figure 5.** Reconstruction of the released rock volume and the entrained glacier volume in the 2017 Piz Cengalo-Bondo landslide cascade. Note that the boundary between the 2011 and 2017 release volumes is connected to some uncertainties, explaining the slight discrepancies among the reported volumes. The glacier volume shown is neither corrected for entrainment related to the 2011 event, nor for glacier retreat in the period 2011–2017.



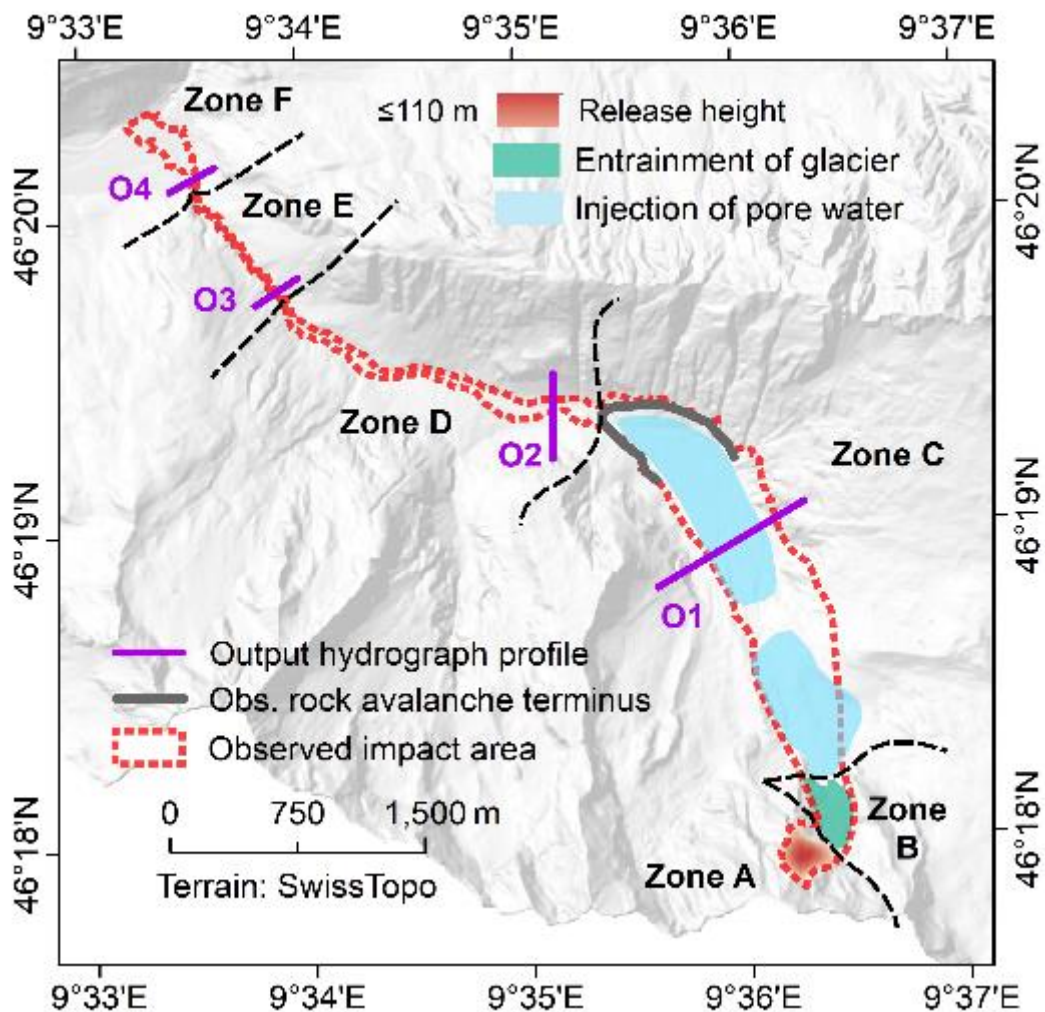
**a) Scenario S1**



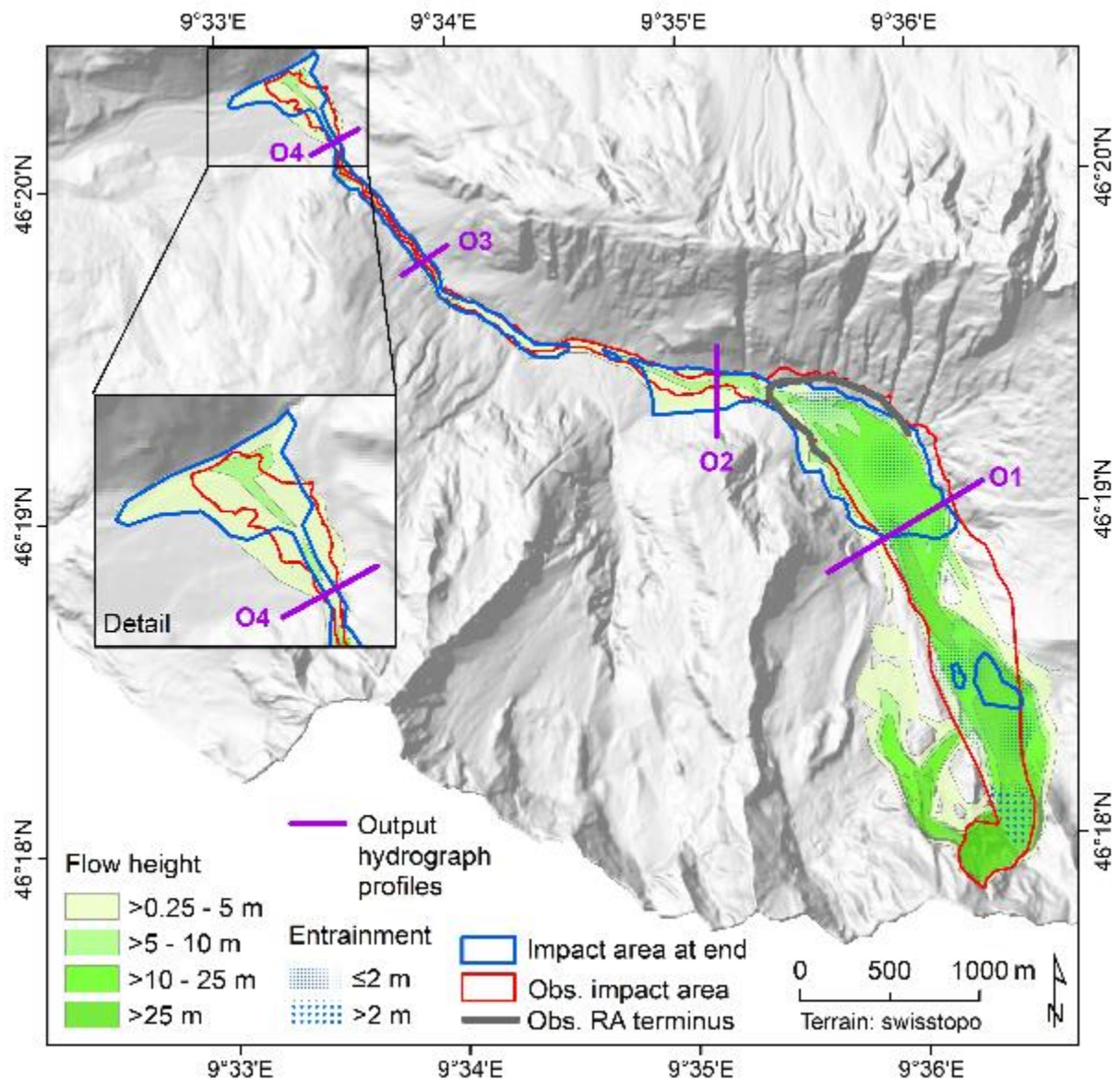
**b) Scenario S2**



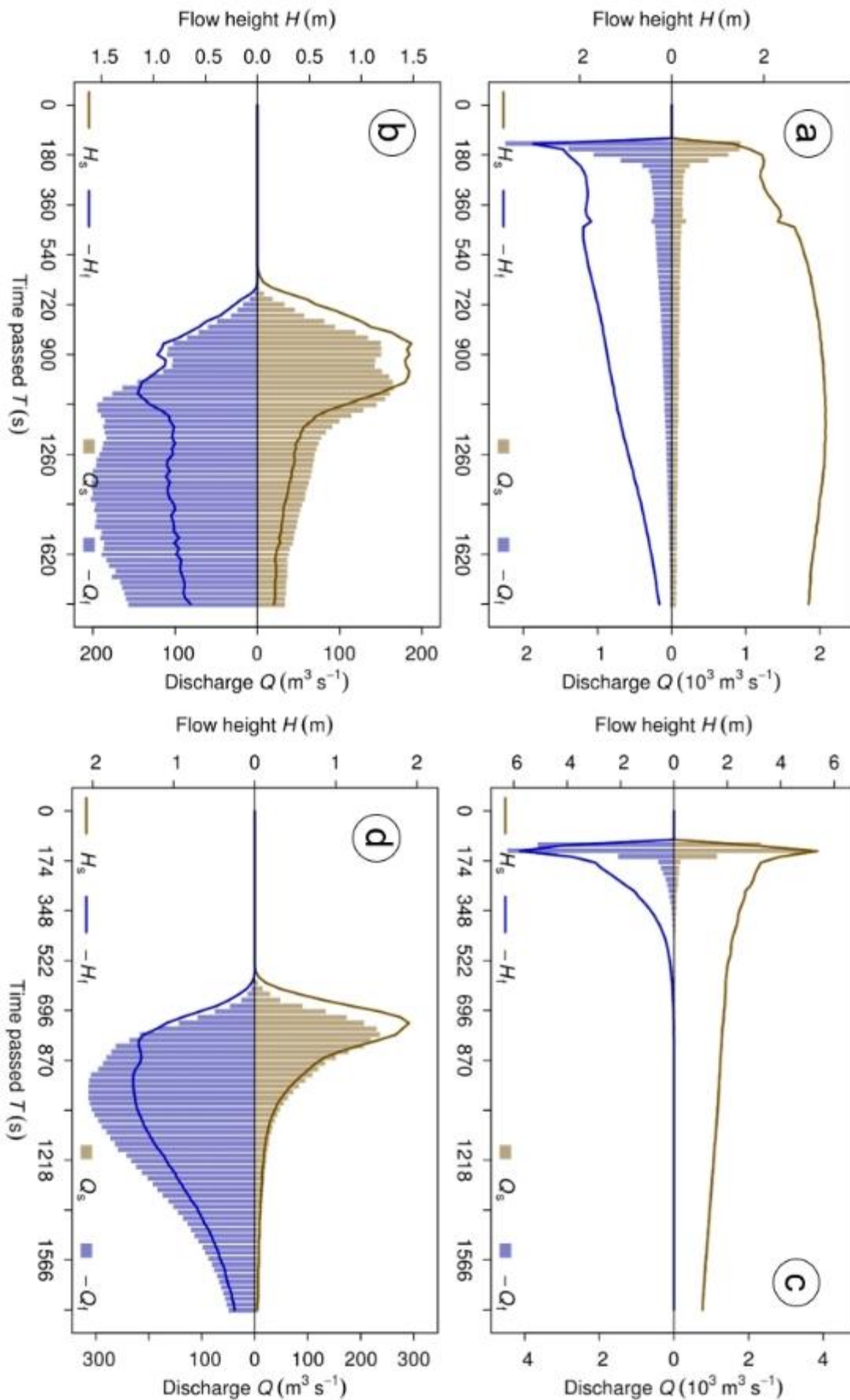
713 **Figure 6.** Qualitative conceptual models of the rock avalanche-debris flow transformation. (a) **Scenario**  
714 **S1**; (b) **Scenario S2**. See text for the detailed description of the two scenarios.  
715



716  
 717 **Figure 7.** Overview of the heights and entrainment areas as well as the zonation performed as the basis  
 718 for the simulation with r.avaflow. Injection of pore water only applies to the Scenario A. The zones A–F  
 719 represent areas with largely homogeneous surface characteristics. The characteristics of the zones and  
 720 the model parameters associated to each zone are summarized in Table 1 and Fig. 4. O1–O4 represent  
 721 the output hydrograph profiles. The observed rock avalanche terminus was derived from WSL (2017).  
 722



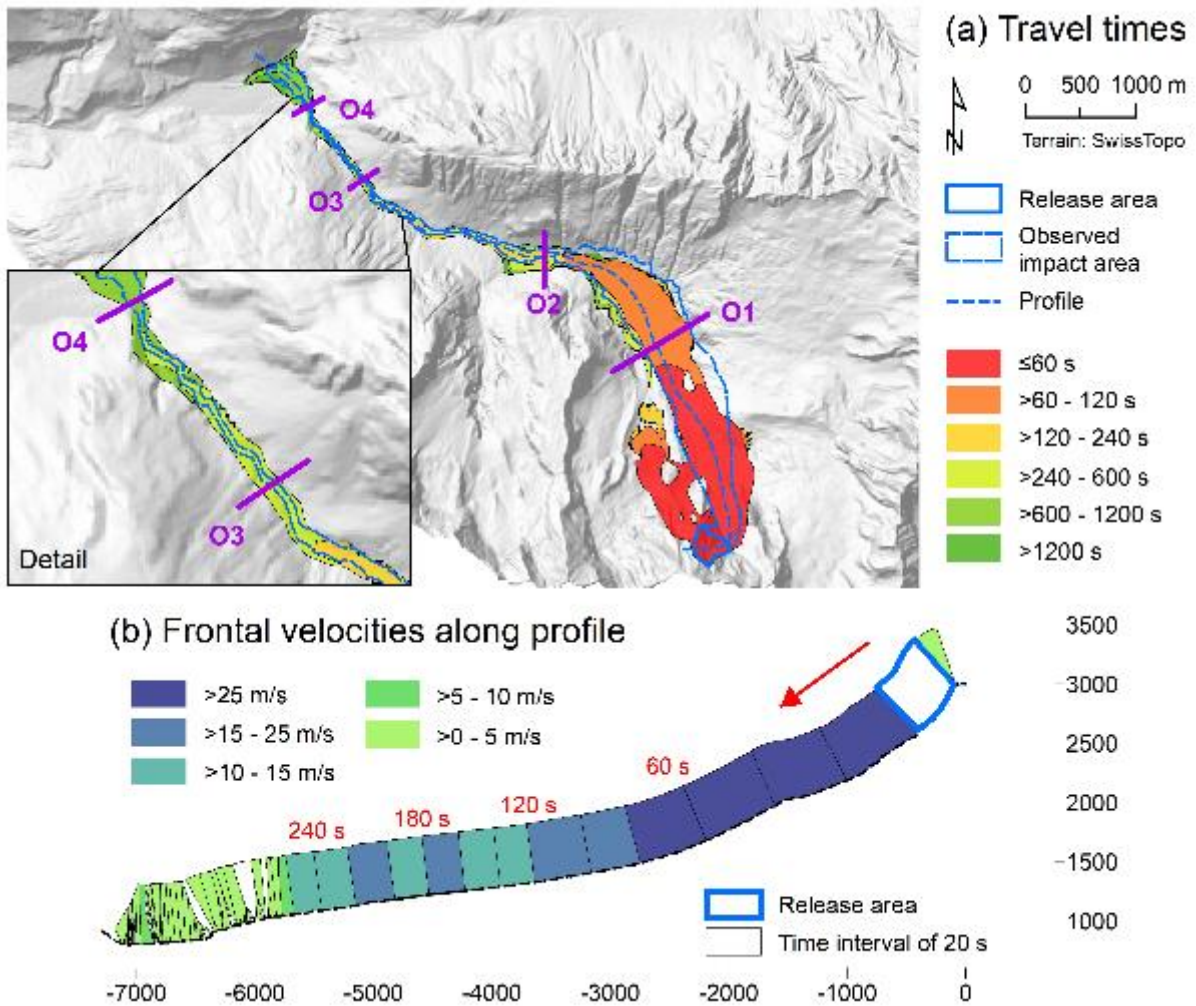
723  
 724 **Figure 8.** Maximum flow height and entrainment derived for **Scenario S1**. RA = rock avalanche; the ob-  
 725 served RA terminus was derived from WSL (2017).  
 726



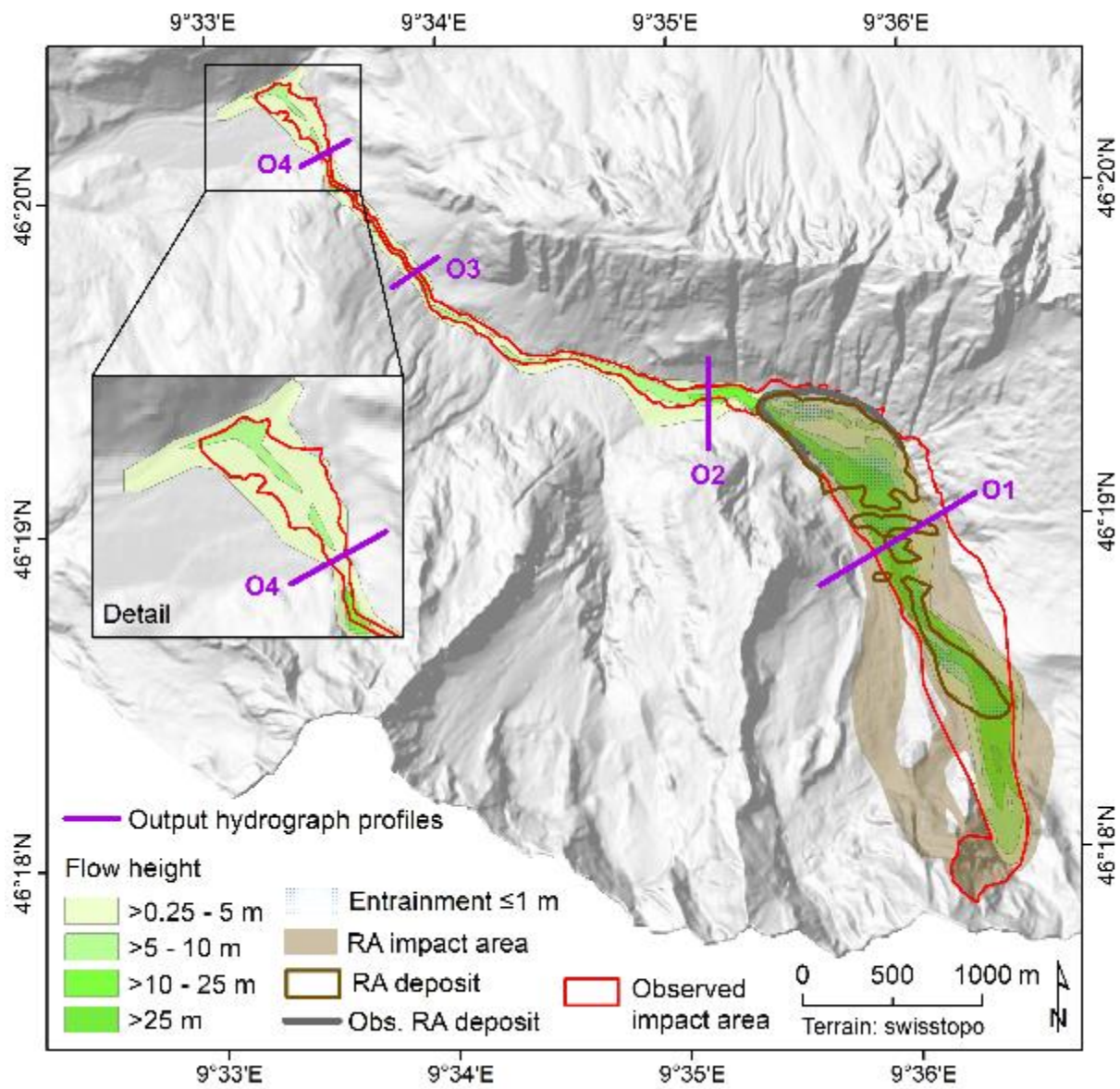
727  
728  
729

Figure 9. Output hydrographs OH2 and OH4 derived for the scenarios S1 and S2. (a) OH2 for Scenario S1. (b) OH4 for Scenario S1. (c) OH2 for Scenario S2. (d) OH4 for Scenario S2. See Fig. 7 and Fig. 8 for

730 the locations of the hydrograph profiles O2 and O4.  $H_s$  = solid flow height;  $H_f$  = fluid flow height;  
731  $Q_s$  = solid discharge;  $Q_f$  = fluid discharge.  
732

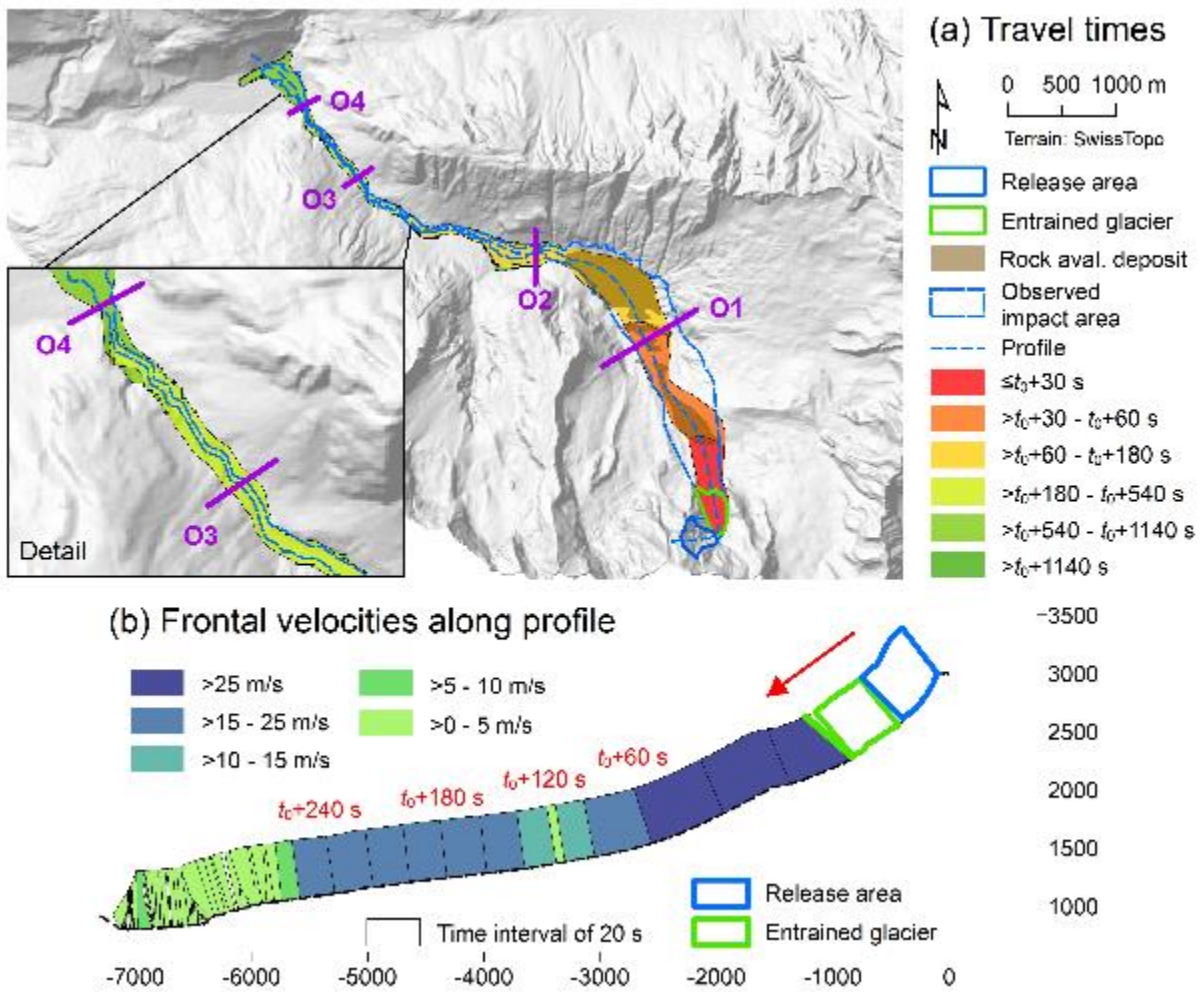


733  
 734 **Figure 10.** Spatio-temporal evolution and velocities of the event obtained for **Scenario S1**. (a) Travel  
 735 times, starting from the release of the initial rock slide-rock fall. (b) Frontal velocities along the flow  
 736 path, shown in steps of 20 s. Note that the height of the velocity graph does not scale with flow height.  
 737 White areas indicate that there is no clear flow path.  
 738



739  
 740 **Figure 11.** Maximum flow height and entrainment derived for **Scenario S2**. RA = rock avalanche; the  
 741 observed RA terminus was derived from WSL (2017).  
 742





743  
744  
745  
746  
747  
748  
749

**Figure 12.** Spatio-temporal evolution and velocities of the event obtained for **Scenario S2**. (a) Travel times, starting from the release of the initial rock slide-rock fall. Thereby  $t_0$  (s) is the time between the release of the rock slide-rock fall and the mobilization of the entrained glacier. (b) Frontal velocities along the flow path, shown in steps of 20 s. Note that the height of the velocity graph does not scale with flow height. White areas indicate that there is no clear flow path.